Universität Osnabrück
Fachbereich Physik

Collective effects and phase transitions in simple Brownian motors

Master-Arbeit
vorgelegt im Rahmen der Prüfung für
den Masterstudiengang Physik von

Gia-Danh Lam
Matrikel-Nummer: 938251

Erstprüfender:
Prof. Dr. rer. nat. Philipp Maaß

Zweitprüfender:
Dr. Marcel Dierl

Osnabrück, February 9, 2016

Abstract

The fluctuating motion of small particles in media caused by random collisions is known as Brownian motion. To molecular motors, this temperature dependent motion can constitute an obstacle. In contrast, Brownian motors exploit this undirected motion in order to rectify motion. The so-called flashing ratchet is a paradigmatic example of a Brownian motor. While the ratchet potential is switched on, particles accumulate at the potential minimum, whereas particles are allowed to diffuse freely, when the potential is switched off. Because of the asymmetric form of the potential, a non-zero current arises from switching the potential on and off, although all forces and gradients are on average vanishing. The working principle of the flashing ratchet is well understood, but a study of the behaviour, when the system is coupled to particle-reservoirs of various densities, has not been conducted yet. In this thesis, the behaviour has been studied and a connection between the flashing ratchet and the ASEP has been found, which is another model of transport. In contrast to the flashing ratchet, the motion of particles is biased by a constant external force. In the ASEP, different so-called boundary-induced phases exist. Analogous same phases, phase transitions and similar collective effects can be found in the flashing ratchet model.

Kurzfassung

Als Brownsche Bewegung wird diejenige fluktuierende Bewegung bezeichnet, die kleinste Teilchen in einem Medium aufgrund von zufälligen Kollisionen ausführen. Diese wärmebedingte Bewegung kann für molekulare Motoren ein Hindernis darstellen. Brownsche Motoren hingegen nutzen genau diese ungerichteten Bewegungen aus, um eine gerichtete Bewegung zu erzeugen. Ein paradigmatisches Beispiel eines Brownschen Motors ist die sogenannte Ein-Aus-Ratsche. Bei eingeschaltetem Ratschenpotential sammeln sich die Teilchen im Potentialminimum, wohingegen die Teilchen frei diffundieren können, wenn das Potential ausgeschaltet ist. Durch die asymmetrische Form des Potentials resultiert aus dem Ein- und Ausschalten ein von Null verschiedener Strom, obwohl alle Kräfte und Gradienten im Mittel verschwinden. Die Funktionsweise der Ein-Aus-Ratsche ist wohl bekannt, jedoch wurde bislang noch nicht das Verhalten bei angekoppelten Teilchen-Reservoiren verschiedener Dichten untersucht. In dieser Arbeit wurde dieses Verhalten untersucht und eine Verbindung zwischen der Ein-Aus-Ratsche und dem ASEP, einem anderen Transportmodell, wurde gefunden. Im Unterschied zum Ratschenmodell wird beim ASEP eine bevorzugte Bewegungsrichtung durch eine externe konstante Kraft vorgegeben. Beim ASEP gibt es verschiedene sogenannte rand-induzierte Phasen. Analoge gleiche Phasen, Phasenübergänge und ähnliche kollektive Effekte können bei der Ein-Aus-Ratsche beobachtet werden.

Contents

1 Introduction

On a microscopic scale, suspended particles in a fluid are in continuous but irregular motion, even without an apparent external force. This phenomenon of erratic motion is called Brownian motion, named after the botanist Robert Brown. During his studies on plants he observed pollen suspended in water. To his surprise, 'dead' pollen grains were still moving. Therefore, in 1827, he has systematically tested in media suspended organic and inorganic particles [Bro66]. A theoretical description and explanation of this phenomenon has not been found until much later by A. Einstein in 1905 [Ein05] and independently by M. Smoluchowski in 1906 [Smo06]. The molecular-kinetic theory of heat by A. Einstein - to the problem of explaining Brownian motion - gives two important results. The first result says that the diffusion coefficient D is dependent on the temperature T and on the mobility of particles μ. The dependency is described by the Einstein-relation, also known as the Einstein-Smoluchowski-relation $D = \mu k_B T$. The second result is the relation between the diffusion coefficient D and the mean-square-displacement (MSD) $\langle x^2(t) \rangle$ in time:

$$D = \lim_{t \to \infty} \frac{1}{2dt} \langle x^2(t) \rangle, \tag{1.1}$$

where d is the space dimensionality.
If it was not for the second law of thermodynamics prohibiting a perpetuum mobile of the second kind, the generation of directed motion by capitalising on the new found temperature-diffusion relation would have been an excellent way to transform ambient heat into mechanical work. In a gedankenexperiment introduced by M. Smoluchowski in 1912 [Smo12] and extended by R. Feynman in 1962 in a physics lecture [FLS77], a hypothetical construct of a ratchet with a pawl on one side connected to a paddle wheel on the other side, known as 'Brownian ratchet', illustrates, why in thermal equilibrium no net motion will occur despite the pawl. Still, this gedankenexperiment also shows the possibility, how Brownian motion can be exploited in a non-equilibrium system to rectify motion, i.e. the rotation of the linkage, which may lift a weight, when the paddle wheel and the ratchet are separately placed in two isolated systems of different temperature.
At that time, realizations of such ratchets could only be found in nature because the development of micro- and nanotechnology had been still in its infancy. E. M. Purcell has given a talk about principles of locomotion at the microscopic scale in 'Life at low Reynolds Number' [Pur77]. He discusses the motion of microorganisms like the Escherichia coli (alias E. coli) bacterium [Ber04]. This bacterium tends to move to regions with higher concentration of nutrients by waving its flagella and while in a nutrient-rich area, it behaves like a Brownian particle. Apparently, a bacterium is not in need of a mechanism to rectify Brownian motion since it can 'outrun' diffusion [Pur77]. But if such a bacterium would shrink to the size of molecules, its propulsion would be negligible in comparison to the influence by diffusion. This may be describable as "walking in a hurricane" [AH02], which is why the suppression of diffusion to some degree may be important at nanoscopic scale.
After intensively studying the molecular motor protein kinesin [RLS$^+$99] of the enzyme class adenosintriphosphatase (a.k.a. ATPase), one realized, in which circumstances Brownian motion can be exploited. The protein kinesin consists of a stalk with two heads. The heads are alternately bound to a microtubule resulting in a restriction of the movement to one dimension [RLS$^+$99]. Although its locomotion is evidently ruled by Coulomb forces, as most kinds of kinesin proteins move in the direction of the 'plus end' of a microtubule, the details of the whole mechanism behind the locomotion are still a topic of research.

Interesting is that there have been approaches, using so called 'Brownian motors' as a model to study alternative mechanisms, where Brownian motion is a crucial factor for a rectified movement of the protein kinesin [AD99].
The term 'Brownian motor' has been mentioned and defined for the first time in 1995 by P. Hänggi and H. Bartussek in ref. [BH95] to distinguish these from molecular motors. It describes a model, where directed motion occurs without a net gradient or a net force. The defining features are stated as follows: An asymmetrical ratchet potential, thermal noise and the driving of the system out of equilibrium by a time-correlated change of the potential landscape or of the noise.
An illustrative and simple example often used to demonstrate, how a Brownian motor works, is the 'flashing ratchet'. Suppose in a one-dimensional system in equilibrium, particles are confined between two maxima in an asymmetric ratchet potential where the well minimum is found near the right boundary. If particles are then allowed to diffuse when the potential is globally set to zero, more particles will pass the position of the right boundary than the position of the left boundary due to the asymmetric density distribution caused by the asymmetric potential. If the potential is switched on and off indefinitely, quasi flashing, then a net transport to the right will occur. This concept first presented by A.L.R. Bug and B.J. Berne [BB87] and independently later by A. Ajdari and J. Prost [AP92] has been realized in 1994 by the latter group in cooperation with J. Rousselet and L. Salome. In their experiment, latex beads have been transported in channels, which are formed by interdigitated Christmas-tree-like electrodes [RSAP94].
There have been many more realizations of different kinds of Brownian motors before and since, albeit not always termed as such. The flashing ratchet is one of the simplest Brownian motors and due to its simplicity, it has already been implemented in or as a device in various fields, whether in the transport and segregation of DNA-oligomers [BHH$^+$99], in nanoarchitectonic computing [AKK$^+$15] or in other devices where pump-like features are necessary. Although the concept of the flashing ratchet is clearly understood, the nature of the model has not been completely grasped. To gain a better understanding of the flashing ratchet model, collective effects and phase transitions of this simple Brownian motor will be numerically analyzed in two dimensions, which enables a better comparability to real systems.

1.1 Outline

In the second chapter, Monte-Carlo methods will be introduced. Especially the Metropolis-algorithm and the kinetic Monte-Carlo method will be discussed in regard to their field of application in the context of equilibrium- and non-equilibrium thermodynamics. Moreover, specific details concerning the simulations are pointed out.
The third chapter is about the asymmetric simple exclusion process (ASEP). First, known properties of the one-dimensional ASEP will be presented. As will be seen later, there are two kinds of approaches to determine the phase diagram of the ASEP. Afterwards, the two-dimensional ASEP, which has been studied in this thesis, will be compared to the one-dimensional ASEP. The chapter concludes with an investigation of a specific phenomenon occurring in the ASEP.
In the fourth chapter, the flashing ratchet is discussed. Comparisons between the ASEP and the flashing ratchet are drawn with respect to collective effects and phase transitions. Lastly, the efficiency and the performance of the flashing ratchet is examined.
In the fifth chapter, the results are briefly summarized and an outlook on open issues and further studies is given.

2 Introduction of Monte-Carlo Methods

In physics, statistical ensembles, introduced by J. Gibbs [Gib02], are essential for studying equilibrium thermodynamics. By statistical ensembles every possible state of a specific system is considered. For example, an equilibrated system with N particles in a volume V in contact with a heat bath of temperature T can be theoretically described by the canonical ensemble (also referred to as NVT-ensemble). Expected values of state variables such as energy, chemical potential or entropy can then be obtained from the canonical partition function, which is defined for a discrete system as

$$Z = \sum_m e^{-E_m/k_B T} = \sum_m e^{-\beta E_m}$$

with the Boltzmann constant k_B, the temperature T and the energy E_m belonging to a microstate m. For a continuous system, it is defined as

$$Z = \frac{1}{h^{3N} N!} \int dqdp \; e^{-\beta \mathcal{H}(q,p)}$$

with the Planck constant h and the Hamilton function $\mathcal{H}$ of the canonical coordinates $q = \{\vec{x}_1,...,\vec{x}_N\}$ and $p = \{\vec{p}_1,...,\vec{p}_N\}$. The probability for the system to be in a microstate m is given by $p(m) = e^{\beta E_m}/Z$, which is known as the (Gibbs-)Boltzmann distribution.
Because it is difficult to find explicit analytical descriptions, it is important to obtain values of state variables via computational methods. One well-known model to describe simple spin systems is the two-dimensional Ising model, where the spins are in a spin-up or spin-down state [Isi25]. Consider a square lattice Λ, where each site i is regarded as a spin s, which can take on the values $\{-1,1\}$ representing the spin's orientation. A spin s_i interacts only with its nearest neighbours via an interaction constant J_{ij} and with a possible external field H. The Hamiltonian is thus given by:

$$\mathcal{H} = -1/2 \sum_{i,j} J_{ij} s_i s_j - H \sum_i s_i$$

The spin system is usually simulated by using so-called 'Monte-Carlo-methods'. Monte-Carlo methods are stochastic means to obtain results based on a vast number of random experiments [GT13]. The expected value of a state variable is obtained approximatively as the sample mean. According to the law of large numbers, this sample mean will converge to the anticipated expected value with increasing number of samples. Certainly, this is only valid if the frequency distribution represented by the samples converges to the desired probability distribution. In order to study systems in thermodynamic equilibrium, like the Ising model, the frequency distribution has to converge to the probability distribution of the desired ensemble so that the independent experiments represent the statistical ensemble. This is achieved by satisfying 'detailed balance', since the system will approach an equilibrium state at long times if 'detailed balance' is fulfilled. This means that the rate of any process is equal to the rate of its reverse process. Mathematically, it can be formulated in terms of Markov processes. For this purpose, first the Markov process will be defined:
Let T be an index set, (Ω,Σ,P) a probability space with a filtration $(\mathcal{F}_t)_{t\in T}$ and $\{m_i\}_{i\in\mathbb{N}}$ a sequence of states. Then, a stochastic process $X = (X_t)_{t\in T}$ adapted to the filtration $(\mathcal{F}_t)$ is said to have Markov property if the equation

$$P(X_{i+1} = m_{i+1}|X_i = m_i,...,X_0 = m_0) = P(X_{i+1} = m_{i+1}|X_i = m_i)$$

holds. Therefore, the probability to find the system in state m_{i+1} depends only on the previous state m_i.
The transition probability between arbitrary states is then described via a matrix P with entries $\mathrm{P}_{ij} = P(X_i = m_i | X_j = m_j)$ and detailed balance is fulfilled if the probability flux from one state to another state is equal to the reverse flux:

$$\mathrm{P}_{ij} p(m_i) = \mathrm{P}_{ji} p(m_j)$$

In terms of Monte-Carlo methods, the chosen rates between two arbitrary states of the system have to satisfy detailed balance. A Monte-Carlo method fulfilling this condition has been provided by N. Metropolis *et al.*, which is known as the Metropolis algorithm [MRR$^+$53]. For the two-dimensional Ising-model, the Metropolis algorithm consists of the following steps:

1. Initialize the system.
2. Choose an arbitrary spin s by generating two uniform random numbers x and y representing the spin's coordinate.
3. Calculate the energy difference ΔE between the system states if the spin is flipped and the current system state.
4. Calculate the transition probability $W(s,s')$ given by $e^{-\Delta E/kT}$ in the canonical ensemble.
5. Generate a uniform random number $z \in [0,1]$.
6. Accept or reject the spin flip in case $z \leq W(s,s')$ or $z > W(s,s')$, respectively.
7. Return to step 2.

The number of iterations, that amounts to the number of spins in the system $|\Lambda|$, is mostly understood as a Monte-Carlo step (MCS) and defines a 'time unit'.
Based on the Metropolis algorithm, more efficient algorithms have been developed and proposed such as the Wolff algorithm or the Swendsen-Wang algorithm. Although the Ising model is quite simple, it is interesting as it exhibits a phase transition in space dimensions greater than one at a critical temperature T_c (, e.g. in two dimensions: see fig. 2.1,) and therefore, it displays a similar behaviour as uniaxial ferromagnetic materials. Besides the model's simplicity, this may be another reason, why the Ising model is a textbook example for simulations in computational physics despite the fact that it has been solved exactly in one and two dimensions analytically.
But since exact analytical results are preferable, computational methods are principally more important in non-equilibrium systems, where a general mathematical theory is not available and thus, analytical tools to describe the system properly may not have been found yet or neglect important details. As stated in the introduction, Brownian motors are non-equilibrium systems. In fact, the majority of real systems are non-equilibrium systems and due to their complexity, the analysis of such systems can be very difficult. Hence, a break down into subsystems or the reduction to simplified models becomes necessary. Even if these subsystems or models may not represent a thermodynamic equilibrium system, they may exhibit stationary states, also referred to as steady states, which characterise a part of the system's behaviour. The asymmetric simple exclusion process is such a simplified model for driven diffusive systems. It is a paradigm for non-equilibrium systems, but it is also sufficiently simple, so that a solely analytical study is possible. Therefore,

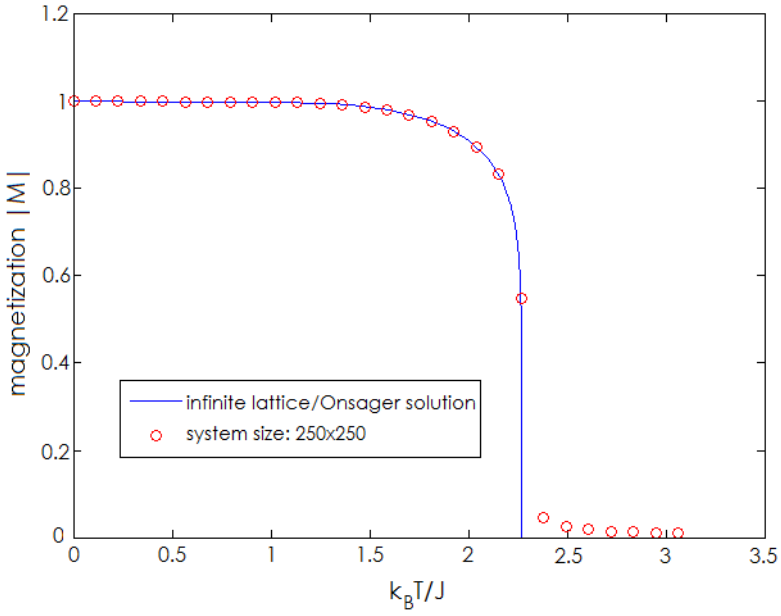

Figure 2.1: First order phase transition in magnetization $|M|$ in the two-dimensional Ising model: An exact solution and results from the Swendsen- and Wang-algorithm are shown. At each temperature point, an average over 1000 MCS has been taken.

the ASEP has piqued the interest of many researchers. Moreover, like the Ising-model, it exhibits phase transitions as will be seen in the next chapter.
Kinetic Monte-Carlo methods are one option to study non-equilibrium systems numerically, although it is also possible to simulate equilibrium systems with these methods. They allow to simulate the correct time evolution of a system, if the processes are independent of each other and of the Poisson-process type. The KMC-method, applied in this thesis to simulate the two-dimensional ASEP and the Brownian motor model, is known as the Bortz-Kalos-Lebowitz (BKL) algorithm [BKL75], though it should have been called the Young-Elcock algorithm, since it has already been presented several years earlier by W. M. Young and E. W. Elcock [YE66]. Another KMC-method, which is in principle the same as the BKL-algorithm, has been formulated by D. T. Gillespie specifically for chemical reactions and it is known as the Gillepsie-algorithm. The BKL-algorithm is divided in the following steps:

1. Initialize the system and set the time to 0.
2. Calculate for all n possible transitions the rates r_i, $i = \{1,...,n\}$, which belong to the transition $i \leq n$. The total rate is denoted as $R_{\text{tot}} = \sum_{i=0}^{n} r_i$.
3. Generate two uniform random numbers $z_1 \in (0,1]$ and $z_2 \in (0,1]$.
4. Find the transition i, where $R_{i-1} < z_1 \leq R_i$ is satisfied, where the relative cumulative rate R_i is defined as $R_i = R_{\text{tot}}^{-1} \sum_{j=0}^{i} r_j$ with $r_0 = 0$.
5. Execute the transition i belonging to the rate R_i and update the time by Δt, which is a function of the rates and the random number z_2.
6. Return to step 2.

There are two remarks about this algorithm. The first remark is about the n transitions in step 2. One may associate with n every possible transitions, but usually it is possible to form classes of transitions Γ_j, also referred to as binning, where m rates $r_i = r_{i+1} ... = r_{i+m-1}$ are subsumed, e.g. the jump rates of particles to a specific direction in a simple system. Then, the cumulative rate R_i has to be redefined as $R_i = \sum_{j=1}^{i} m_j \Gamma_j$ and another step consisting of randomly choosing one of the m_j transitions has to be included. Secondly, the rates r_i can be time-dependent or time-independent. If the rates are time-independent, then each rate r_i can be viewed as constants until the next iteration and the time increment Δt can be readily calculated as:

$$\Delta t = -R_{\text{tot}}^{-1} \ln z_2 \tag{2.1}$$

But in case of time-dependent rates, e.g. the rates in the Brownian motor model, the time increment Δt has to be found from the equation:

$$\int_{t'}^{t'+\Delta t} \sum_{i=1}^{n} r_i(t) \mathrm{d}t = -\ln z_2 \tag{2.2}$$

Generally, there are some effects in computer simulations to be kept in mind. First, before beginning measurements, transient times have to be considered to let the system evolve and approach a stationary state of the system. But in the case that the intent might be to follow the evolution of a system into a stationary state, the very transient times may be of interest. Another effect is the so-called finite-size effect occurring due to the unavoidable finite size of the system. The difference between the analytical result and the result from a Monte-Carlo simulation shown in fig. 2.1 is caused by the finite-size effect. This difference is reduced if the size of the system is enlarged. The size of the system in the ASEP and the Brownian motor model may also have an impact on the results if it is chosen too small. Lastly, the simulation time needs to be very long since the accuracy of the results obtained with Monte-Carlo methods is based on the law of large numbers.

3 ASEP

The asymmetric simple exclusion process is an important model for transport processes and as a simple model, modifications can be easily integrated in order to adapt it to a more complex model. Conversely, transport models, including Brownian motors, can be reduced to the ASEP, though it might be an oversimplification. But for this reason, the relation between the flashing ratchet model and the ASEP will be examined and thus, a fundamental understanding of the ASEP is necessary. The discussion of the ASEP in this chapter is divided into two parts. First, the ASEP will be introduced and basics of the one-dimensional ASEP will be presented. Then, the two-dimensional ASEP, which has been studied here, will be discussed, to allow a direct comparison between the two-dimensional model of the flashing ratchet and the ASEP.

3.1 Basics to ASEPs in One Dimension

3.1.1 The Simple Exclusion Process

In general, the ASEP is a particular case of the simple exclusion process (SEP). The SEP is a stochastic process of an interacting particle system with simple hard-core repulsion interaction. Consider a lattice $\Lambda \subset \mathbb{Z}^d$, where a site $x = \{x_1,...,x_d\} \in \Lambda$ can be occupied or vacant, which is expressed by $\{1\}$ and $\{0\}$ respectively. If the occupation number of a site is denoted by n_x, the state of the system S is completely described by the configuration $\{n_x | x \in \Lambda\}$. When the lattice is finite, the state space $\{S_i | S_i \neq S_j\}$ is also finite and the SEP can be described as a continuous-time Markov chain of transitions $S_i \to S_{i+1}$. Generally, the condition that the target state is only allowed to differ by a single exchange of occupation numbers of neighbouring sites including at least one occupied site is postulated. Put differently, a particle occupying one site can only jump to a neighbouring vacant site and will otherwise have to rest, which is equivalent to swapping states with a neighbouring occupied site. A transition is stochastically triggered by introducing exponential waiting times with mean 1 for each occupied site. Hence, the SEP belongs to the class of Poisson processes, which describes stochastic processes with independent increments, i.e., the exponential distributed waiting time is memoryless [Spi70].
The ASEP has been first defined in 1968 by C.T MacDonald *et al.* to describe protein synthesis by ribosomes of different lengths L on a m-RNA template [MGP68]. This research group has already solved the ASEP, i.e. $L = 1$, by means of mean-field theory and discussed and presented the results for the phase diagram and the current-density relation. Independently, the ASEP has been introduced by F. Spitzer in 1970 as a model for an interacting particle system [Spi70]. A very similar model but with a parallel update instead of a sequential update of the particles is the Nagel-Schreckenberg-model, proposed to simulate freeway traffic. They have studied the interdependence between traffic jams and 'car'-density. The similarity of the empiric results and the simulation results for the flow of cars shows that their model does capture real situations well, although it is a highly simplified model [NS92].
The ASEP can be diversely defined in regard to the choice of dimensions, the bias of the jump rates and the boundary conditions. The original ASEP model is a system in one dimension, thus allowing only jumps 'to the left' or 'to the right' with either periodic or open boundary conditions [MGP68]. In one dimension, the jump rates are usually denoted as p for the right direction and as q for the left direction with the condition $p,q \geq 0$. In studies concerning the ASEP, one either finds that the condition $p + q = 1$ (a) is satisfied

or that p is set to 1 for $q \geq 0$ (b) inducing a time rescale of the mean waiting time to $1/(p+q)$ [Sch01]. Moreover, different denotations have been used for identical models. In the literature, one will find in most cases, if q is set to zero, that the model is termed either ASEP or totally asymmetric SEP (TASEP). Accordingly for $q > 1$, the model is usually either termed partially asymmetric SEP (PASEP) or simply ASEP. From here on out, the latter description of both cases will be used, that is to say TASEP for $q = 0$ and ASEP for $q > 1$ while condition (a) is satisfied. The model is denoted as a symmetric SEP (SSEP) for $p = q = 1/2$, which is the only choice of p and q describing an equilibrium system. In systems of higher dimensions d, jump rates p_i and q_i can be introduced, where $i = \{1,...,d\}$ refers to the respective space dimension. The last specification, the choice of the boundary conditions, affects essentially the dynamics of the system. Two boundary conditions will be presented and discussed. These are:

1. only periodic boundary conditions: bulk system
2. open boundary condition: open system

In the bulk system, the number of particles N is conserved. The dynamics are only dependent on the jump rates and the density of particles $\rho = N/(|\Lambda|)$. The open system is realized via couplings to reservoirs with variable particle densities. In one dimension, usually two reservoirs are inserted at the left and right boundary respectively. This model has been studied in-depth and extensively. In higher dimensions, the model can become more complex and more diverse. The interactions in the system may become non-trivial since the particle density of each reservoir can be chosen freely. An alternative option consists of using periodic and open boundary conditions in differing space dimensions. It may only yield the same behaviour as the model reduced by the dimensions, where periodic boundaries are imposed, however, characteristics in specific quantities may only be observable in the 'original' model.
In the following, an overview of fundamental works on (T)ASEPs will be presented. The discussion is restricted to the one-dimensional ASEP. For convenience, the sites will be represented by the variable $i = 0,...,N$ ascending from left to right.

3.1.2 Analytical Approaches

Given that the ASEP is a model of particle transport, the current J and for an open system also the average occupation number $\langle n(i)\rangle = \rho(i)$ are of interest. Generally, the correlation between different sites have to be studied, since it is possible to derive the density $\rho(i)$ and the current J from these correlations [DDM92].
The current-density relation can be easily determined in the bulk system. In the bulk system every configuration is equally probable, since no site $i \in \Lambda$ is singular and the number of particles is conserved. Therefore, the density $\rho(i)$ is uniform and equals the bulk density ρ_b, which is the density at sites far from the boundaries and will be denoted in the bulk system as ρ. From this it follows, that the equation

$$\langle s_i s_{i+1} ... s_j \rangle = \langle s_i \rangle \langle s_{i+1} \rangle ... \langle s_j \rangle \tag{3.1}$$

([DDM92]) and also the equation

$$\langle s_i \rangle = \langle s_j \rangle = \rho \quad i,j \in 1,....,n \tag{3.2}$$

hold and the current J is readily to be calculated. It can be written as [MGP68]:

$$\langle J \rangle = p\langle s_i(1 - s_{i+1})\rangle - q\langle s_{i+1}(1 - s_i)\rangle$$

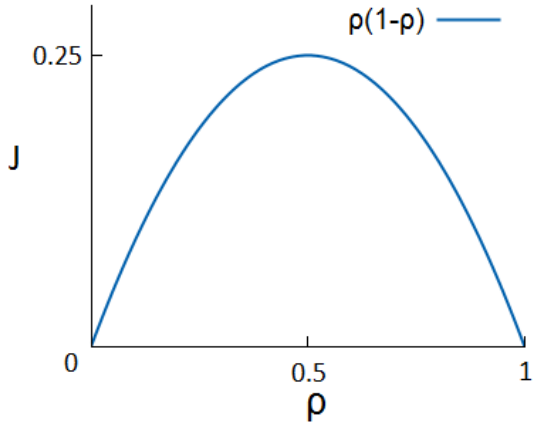

Figure 3.1: Current-density relation of the TASEP with $J_{max} = 1/4$ for $\rho = 1/2$, $p = 1$ and $q = 0$.

and with eqs. (3.1) and (3.2) it becomes

$$J = (p - q)\rho(1 - \rho) \tag{3.3}$$

The current-density relation for the TASEP is shown in fig. 3.1. Although, in ref. [MGP68] by C.T. MacDonald *et al.*, mean-field results neglecting correlations of higher order have already been presented, an exact analytical approach for the open system has been proposed only several years later.
The first exact approach for the TASEP with injection and ejection rates α and β has been given by B. Derrida, E. Domany and D. Mukamel and is based on recursion [DDM92]. To calculate specific quantities in the steady state, a probability distribution P_n for every possible system configuration $(s_1,...,s_n)$ with $s_i = \{0,1\}$ is introduced. This probability distribution is expressed via a weight function f_n and a normalization factor Z_n:

$$P_n(s_1,...,s_n) = f_n(s_1,...,s_n)/Z_n, \tag{3.4}$$

where Z_n is defined as

$$Z_n = \sum_{s_1=0,1} ... \sum_{s_n=0,1} f_n(s_1,...,s_n)$$

Their recursion rule is only applied to the weight function f_n and is rather complex, so that a calculation can become very laborious depending on the choice of n, α and β. For $\alpha + \beta = 1$ (c), they have found that the correlation between different sites decomposes, thus eq. (3.1) holds. From this it follows that the mean field results are exact if (c) is true. Since in this case the density is uniform and fixed by $\langle s \rangle = \alpha = 1 - \beta$, the open system can be considered as the bulk system with the bulk density $\rho_b = \langle s \rangle$. Therefore, the current is given by eq. (3.3) with $\rho = \rho_b$, as has been obtained by mean-field theory.
If f_n is known, the average occupation number $\langle s_i \rangle$ can be calculated with the following equation:

$$\langle s_i \rangle = \sum_{s_1} ... \sum_{s_n} s_i f_n(s_1,...,s_n)/Z_n \tag{3.5}$$

In ref. [DDM92], an example has been given for $\alpha = \beta = 1$, to show how the recursion method can be applied for specific values of the injection and ejection rates α and β. The presented phase diagram in ref. [DDM92], which is similar to the phase diagram in fig.

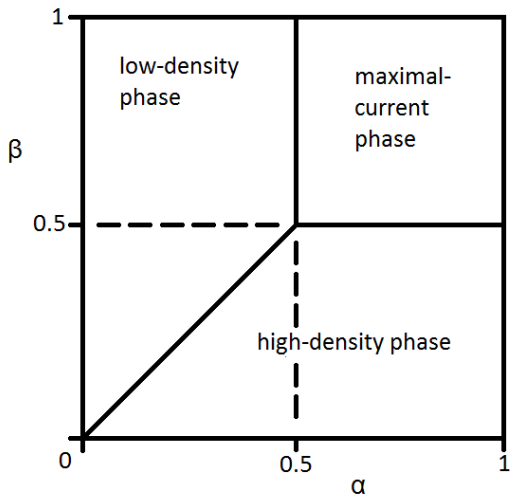

Figure 3.2: Phase diagram of the TASEP: 1) high-density phase for $\alpha > \beta$ and $\beta < 1/2$, 2) low-density phase for $\alpha < \beta$ and $\alpha < 1/2$, 3) maximal-current phase for α,$\beta \geq 1/2$, 4) coexistence line for $\alpha = \beta < 1/2$; boundaries between subphases are marked as dashed lines.

3.2, has been determined by means of mean-field theory. The phase of the system in a steady state is depending on the injection rate α and the ejection rate β (cf. fig. 3.2). There are overall three phases, consisting of a low-density (LD) phase, a high-density (HD) phase and a maximal-current (MC) phase. In addition, there exists a coexistence (CE) line separating the low-density phase and the high-density phase, where the density profile exhibits a fluctuating shock front [DDM92]. Further calculations and a more elaborate discussion about the phases and phase transitions have been done by E. Domany and G. Schütz. They also provided a closed expression of the aforementioned recursion formula and showed that the high- and low-density phase can respectively be separated in two subphases. The subphases are separated by the boundaries, where the injection or the ejection rate transcends a threshold so that either $\langle s_i \rangle > 0.5 \; \forall \; i$ in the high-density phase or $\langle s_i \rangle < 0.5 \; \forall \; i$ in the low-density phase no longer holds [SD92]. This matter is revisited later in ch. 3.1.3.
A different approach is the so called 'matrix product ansatz', which has been proposed by B. Derrida *et al.* to solve the TASEP [DEHP93]. Before, the matrix ansatz has already been applied to the problems of directed lattice animals [HN93] and spin chains [FNW92, KSZ91]. According to ref. [DEHP93], the weight function f_n can be written in the form

$$f_n = \langle W | \prod_{i=1}^{n} (Ds_i + E(1 - s_i)) | V \rangle \tag{3.6}$$

if the 'bra'-vector W and 'ket'-vector V and the matrices D and E satisfy the following conditions:

$$DE = D + E \tag{3.7a}$$

$$\langle W | (\alpha E) = \langle W | \tag{3.7b}$$

$$(\beta D) | V \rangle = | V \rangle \tag{3.7c}$$

In the expression for the weight function f_n in eq. (3.6), the system configuration itself

phase	LD phase	HD phase	MC phase
current J	$\alpha(1-\alpha)$	$\beta(1-\beta)$	$1/4$
bulk density ρ_b	α	$1-\beta$	$1/2$

Table 1: Results of the current J and the bulk density ρ_b in the different phases [DDM92].

is displayed, as an occupied site is represented by a matrix D and an unoccupied site is represented by a matrix E. The normalization factor Z_n can be written as $Z_n = \langle W|C^n|V\rangle$ by introducing the matrix $C = D + E$ because $C^n = (D + E)^n$ includes every possible configuration of D and E. Important to note is that D and E only commute if the condition (c) is satisfied. Otherwise D and E are infinite matrices, which indicates that it may not be trivial to calculate f_n. For a configuration (s_1,...,s_n), the probability distribution P_n is thus given by

$$P_n = \langle W| \prod_{i=1}^{n} (Ds_i + E(1 - s_i))|V\rangle / \langle W|C^n|V\rangle \tag{3.8}$$

and the mean occupation number $\langle s_i\rangle$ by

$$\langle s_i\rangle = \langle W|C^{i-1}DC^{n-i}|V\rangle / \langle W|C^n|V\rangle \tag{3.9}$$

The two-point-correlator $\langle s_i s_j\rangle$, for $i < j$, is defined similar to eq. (3.9). For the TASEP, the current J is calculated by the following two-point-correlator:

$$\begin{aligned} J = \langle s_i(1 - s_{i+1})\rangle &= \frac{\langle W|C^{i-1}DEC^{n-i-1}|V\rangle}{\langle W|C^n|V\rangle} \\ &= \frac{\langle W|C^{i-1}(D + E)C^{n-i-1}|V\rangle}{\langle W|C^n|V\rangle} \\ &= \frac{\langle W|C^{n-1}|V\rangle}{\langle W|C^n|V\rangle} \end{aligned} \tag{3.10}$$

The results of the matrix-product ansatz are confirming the phase diagram obtained from the mean-field calculations in ref. [DDM92]. Especially, the expressions for the current and the bulk density in the different phases have been verified (see. tab. 1). The only difference between the mean-field results and the exact matrix-approach results appears around the coexistence line separating the HD-phase from the LD-phase. The exact results predicts a linear increase of density, whereas the mean-field approach predicts a step-like jump in the density profile. The reason for this difference is that the superposition of this jump being at any arbitrary site is only reflected in the exact results [DEHP93].
The matrix-product ansatz can be applied to the ASEP and to the TASEP with additional second class particles. Since the ASEP includes backward jumps, the conditions (3.7), considering now γ (δ) as the ejection (injection) rate at the left (right) boundary, need to be adapted:

$$pDE - qED = D + E \tag{3.11a}$$

$$\langle W|(\alpha E - \gamma D) = \langle W| \tag{3.11b}$$

$$(\beta D - \delta E)|V\rangle = |V\rangle \tag{3.11c}$$

The weight function in eq. (3.6) is not affected.

One expansion of the ASEP-model is represented by the introduction of additional second-class particles. In this case, also the eq. (3.6) needs to be adapted. In the matrix formulation, a new matrix A needs to be introduced, which describes the second-class particles [DEHP93]. One specification of the dynamics for this model is given by the following update rule. The second-class particles are treated as particles when they jump to unoccupied sites and they are treated as 'holes' in transitions involving first-class particles. If this rule holds, the weight function is given by

$$f_n = tr(X_1...X_n) \tag{3.12}$$

where $X_i = \{D,E,A\}$. If A is defined as $A = DE - ED$, the conditions, that the matrices D, E and A have to satisfy, are:

$$DE = D + E \tag{3.13a}$$

$$DA = A \tag{3.13b}$$

$$AE = A \tag{3.13c}$$

Second class particles are useful to investigate the shock, which occurs in the open system on the coexistence line [DJLS93].
Because of the fact, that the ASEP is similar to other models like the XXZ spin chain or growth models, well known approaches to solve the respective problems like the Bethe-ansatz or the mapping of the ASEP onto the Kardar-Parisi-Zhang (KPZ) equation have been applied to solve the TASEP or ASEP with periodic or open boundary conditions [GM06].

3.1.3 Physically Motivated Approaches

A rather physically inspired approach to determine the steady state of a (T)ASEP is the application of the extremal-current principle:

$$J = \begin{cases} \max\limits_{\rho\in[\rho_r,\rho_l]} J(\rho) & \rho_l > \rho_r \\ \min\limits_{\rho\in[\rho_l,\rho_r]} J(\rho) & \rho_l < \rho_r \end{cases} \tag{3.14}$$

J. Krug proposed the maximal-current principle for the TASEP with open boundary conditions [Kru06], where only the density of the reservoir at the left boundary ρ_l has been altered and the density at the right boundary ρ_r has been kept to zero ($\beta = 1$). This principle has been extended to the extremal-current principle by V. Popkov and G.M. Schütz [PS99], where arbitrary densities for the reservoirs at the left and right boundaries are considered. The extremal-current principle can be readily understood by taking three conditions into account:

1. If the system is in a steady state, the current J is time-independent, that is to say $dJ/dt = 0$.

2. Kirchoff's-rule has to be satisfied. This means that the particle current 'into' a site equals the particle current 'out' of this site.

3. The total current J at any site is composed of the systematic current $J_{\text{sys}}(\rho)$ and the diffusion current $J_{\text{diff}}(k,\rho')$. Here, the spatial derivation is denoted by $'$.

The systematic current J_{sys} is given by the current-density relation obtained from the bulk system, whereas the current J_{diff} results from Fick's law of diffusion ($J_{\text{diff}} = -D\partial\rho/\partial i$). The first two conditions ensure that the current is uniform and will not change in time and with the help of the third condition, the steady state of a system can be determined. In the following, all phases will be discussed. The path, of how the phases are passed through, is schematically shown in fig. 3.3.
Consider a starting point in the phase diagram with $0.5 > \rho_l > \rho_r$ (LD1), which is a point in the LD-phase. If the jump rate q equaled the jump rate p, then the system would be described only by Fick's law and the density would hence decrease linearly with $(\rho_l - \rho_r)/L$, where L is the length of the system. In the (T)ASEP, the non-uniform systematic current J_{sys} (cf. fig. 3.1) will be added to the diffusive current J_{diff} and thus the current near the left boundary would be significantly higher than the current at the right boundary due to the condition $0.5 > \rho_r > \rho_l$. This means, that Kirchhoff's-rule would be violated since the current is not uniform, which violates stationarity. Consequently, to decrease the current at the left boundary and increase the current at the right boundary, the density-gradient at the left boundary has to increase (to zero) and has to decrease further at the right boundary. Therefore, the bulk density approaches the density of the left reservoir ρ_l and a sharp drop of the density is found at the right boundary.
Now, if ρ_r is increased, this drop will diminish until $\rho_l = \rho_r$. In this case, the density and the current J_{sys} are uniform and J_{diff} is zero. Until this point, the maximum-current principle has held true. If ρ_r is further increased, the minimum-current-principle has to be applied (LD2), since the density at the right boundary ρ_r exceeds the density at the left boundary ρ_l. It will be briefly shown that the maximum-current principle would not lead to a steady state which satisfies the above stated conditions. Assuming the bulk density would, with further increase in ρ_r, start to approach ρ_r, then a rise of density has to occur at the left boundary. According to the current-density-relation, the systematic current J_{sys} is in this situation higher at the right boundary than at the left boundary and in addition, due to the rise of the density at the left boundary, the current J_{diff} would

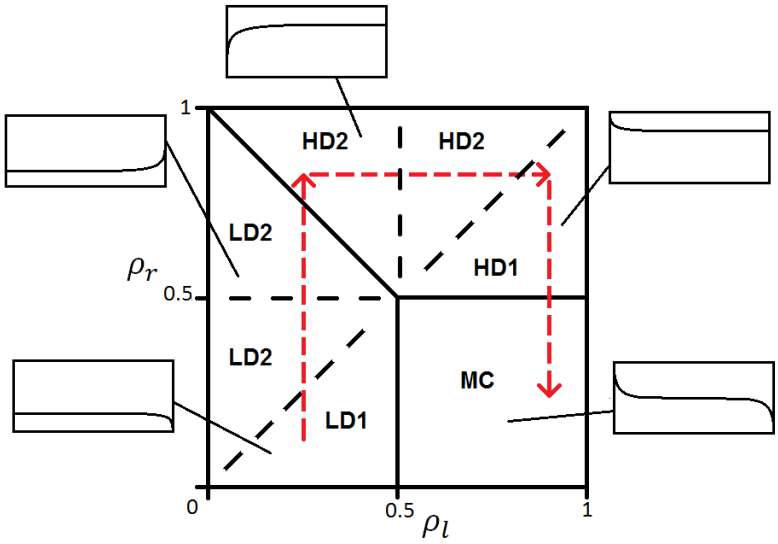

Figure 3.3: Phase diagram of the (T)ASEP with $\rho_l \hat{=} \alpha$ and $\rho_r \hat{=} 1 - \beta$: The path in the phase space, which is followed, is marked by the arrows. Schematic density profiles to the corresponding phases are depicted outside the phase diagram.

be negative at the left boundary and consequently, the current J would not be uniform. Therefore, the bulk density's behaviour has to remain the same ($\rho_b \approx \rho_l$) while a rise at the right boundary forms if ρ_r is increased. According to the current-density relation in fig. 3.1, two important parameter points will be passed through when the density ρ_r is further increased. First, if ρ_r transcends the value 0.5, then there exists a site i at the right boundary, where the systematic current J_{sys} is higher than in its environment. This induces an inflection point in the density profile and therefore, the form of the rise changes distinctly. Secondly, eventually the currents $J_{\text{sys}}(\rho_r)$ and $J_{\text{sys}}(\rho_l)$ have to be equal when $\rho_r = 1 - \rho_l$ holds. Thus, it is possible that the bulk density ρ_b approaches either ρ_l or ρ_r. Since neither steady state is favored, the two phases (LD-phase and HD-phase) coexist.
If now $\rho_r = 1 - \rho_l$ holds, a further increase in ρ_r will lead to a decrease in $J_{\text{sys}}(\rho_r)$ and the situation reverses (HD2). This means that a rise of density at the left boundary is now supported by the minimum-current principle as ρ_l is still smaller than ρ_r. The reasoning is the same as before: If a rise of density formed at the right boundary, the current J at the right boundary would decrease by J_{diff}, while J_{sys} is already smaller at the right boundary than at the left boundary, so that as the result J would not be uniform. Thus, the bulk density ρ_b approaches the density ρ_r. From this point on only ρ_l will be increased. The next important parameter points in the phase diagram are similar to the parameter points in the LD-phase. These are $\rho_l = 0.5$, at which the form of the density rise changes due to an additional inflection point, and $\rho_l = \rho_r$ because from this point on the maximum-current-principle is effective, since $\rho_l > \rho_r$ holds. The reason, that the bulk density stays the same and the rise becomes a drop, when $\rho_l > \rho_r$ holds, is essentially the same as in the transition from LD1 to LD2.
The current parameter point in the phase diagram is described by $\rho_l > \rho_r > 0.5$, which lies in the high-density-phase HD1. If now the density at the right boundary is decreased to 0.5, the bulk density and the current will be $\rho_b = 0.5$ and $J = 1/4$ respectively. A further decrease in ρ_r will, according to the maximum-current principle, result in a drop of density on both boundaries, since the current J is maximized for $\rho = 0.5 \in [\rho_r,\rho_l]$. If the bulk density would still approach ρ_r, then the gradient at a site i with $\rho_i = 0.5$ would be positive and the current at this site would be higher than at the right boundary and the uniformity of the current J would be violated.
All three phases have now been discussed and reasoned by the extremal-current principle in respect of the current-density relation shown in fig. 3.1. A more complex example can be found in ref. [PS99]. Also the domain wall theory presented by G. M. Schütz *et al.* [KSKS98] was echoed in the aforesaid ref. [PS99].
The domain wall theory is a different physically motivated approach, which illustrates the movement of domain walls separating two phases, which have been above referred to as 'drops' and 'rises' of density. The idea behind this theory can be understood by considering the following situation. If one assumes that α and β are sufficiently small, so that the system always reaches a stationary state before another particle enters or exits, then, the domain wall moves by a particle's unit to the left if one particle is injected and it moves by a particle's unit to the right if a particle is ejected. Generalized, the domain wall moves to the left with rate α and moves to the right with rate β, which is expressed by the domain wall velocity $V = \beta - \alpha$. This means that, if $\beta > \alpha$ ($\beta < \alpha$) holds, the parameter point lies in the LD (HD) or in the maximum-current phase, as the domain wall moves to the right (left) boundary. This roughly explains the phase diagram. A more sophisticated argumentation can be given with the help of the continuity equation, but it leads to the same result for the domain wall velocity [KSKS98]. For a detailed discussion and a sophisticated argumentation, reviewing ref. [KSKS98] is recommended.

3.2 ASEP in Two Dimensions

3.2.1 The Model

In accordance with the description in ch. 3.1.1, where the simple exclusion process is outlined, the two-dimensional system consists of a discrete square lattice $\Lambda \subset \mathbb{Z}^2$ with length L and width W. A site (x,y), with $0 \leq x < L$ and $0 \leq y < W$, can be in the state 'occupied' or 'vacant' denoted by $\{1\}$ or $\{0\}$ respectively. To facilitate the description of the system, the denotations row and column are used, which refer to the sites with the same y-coordinate or with the same x-coordinate respectively. Particles in this system may only move up, down, right or left to a neighbouring square. In the case that periodic boundary conditions are chosen at all four boundaries, the lattice can be illustrated by mapping it onto a torus, where toroidal coordinates replace x-coordinates and poloidal coordinates replace y-coordinates. In the open system with periodic boundary conditions at the top and at the bottom boundary and with open boundary conditions at the left and at the right boundary, the system can be illustrated by mapping the lattice onto a cylinder, where the reservoirs are found at the ends (see fig. 3.4). In general, the two-dimensional ASEP differs from the one-dimensional ASEP in regard to the possibility that a particle is able to circumvent another particle.
The energy of the system is given by the following Hamiltonian

$$\mathcal{H} = -V \sum_{x=0}^{L} x \; n(x,y), \tag{3.15}$$

where $n(x,y)$ represents the occupation number at (x,y) and V the potential difference in the x-direction. The transition rates are denoted as $p_{\rightarrow}$, $q_{\leftarrow}$, $p_{\downarrow}$ and $q_{\uparrow}$ and they represent the rates for a particle to jump right, left, down and up respectively. For the said rates Glauber-rates are employed because Glauber-rates ensure that the conditions $1 > p,q \geq 0$ and $p + q = 1$ are satisfied. Thus, the rates are given by:

$$p_{\rightarrow} = (1 + e^{-V/k_B T})^{-1} \tag{3.16a}$$

$$q_{\leftarrow} = (1 + e^{+V/k_B T})^{-1} \tag{3.16b}$$

$$p_{\downarrow} = (1 + e^{-F/k_B T})^{-1} \tag{3.16c}$$

$$q_{\uparrow} = (1 + e^{+F/k_B T})^{-1} \tag{3.16d}$$

The parameter F represents the influence of a possible potential perpendicular to V, but it is in general set to zero unless explicitly stated otherwise. k_B is the Boltzmann constant and T the temperature.
In the above stated open system, four additional rates have to be taken into account. These

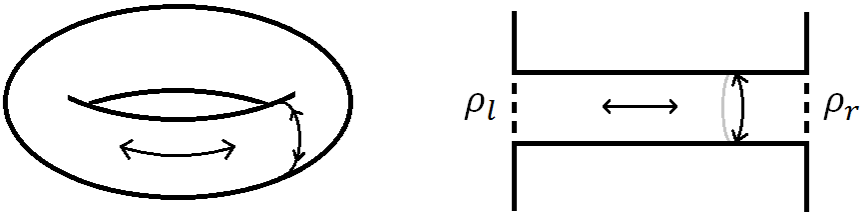

Figure 3.4: Illustration of the models: left) bulk system; right) open system.

are the injection and ejection rates $\Gamma_{\{L,R\},\{\text{in,e}\}}$ at the left and right boundary respectively. In addition to the parameter V, the parameters α and β with $0 < \alpha,\beta < 1$ have to be included:

$$\Gamma_{L,\text{in}} = \alpha(1 + e^{-V/k_BT})^{-1} \tag{3.17a}$$

$$\Gamma_{L,\text{e}} = (1 - \alpha)(1 + e^{+V/k_BT})^{-1} \tag{3.17b}$$

$$\Gamma_{R,\text{in}} = (1 - \beta)(1 + e^{+V/k_BT})^{-1} \tag{3.17c}$$

$$\Gamma_{R,\text{e}} = \beta(1 + e^{-V/k_BT})^{-1} \tag{3.17d}$$

The simulation method is the BKL-algorithm, which has been introduced in ch. 2. For convenience, k_BT has been set to one. Details about the used parameter set are stated in the respective results.

3.2.2 Comparison: 1D ASEP and 2D ASEP

First, the current-density relation will be discussed, since a similar current-density relation will yield, according to the extremal-current principle, a similar phase diagram. In one dimension, the current-density relation is given by eq. (3.3). To verify this equation for the two-dimensional ASEP, the spatially and time-averaged current has been determined. The current in the x-direction has been measured by counting jumps to the left (n_l) and to the right (n_r). Therefore, the current is calculated as follows:

$$J = \frac{n_r - n_l}{WLt_{\text{average}}} \tag{3.18}$$

The case of $F \neq 0$ has also been examined to affirm that in the bulk system the current-density relation holds true on either axis. The results for the currents are shown in fig. 3.5. In comparison of the exact result given by the equation (3.3) to the results obtained from KMC-simulations, there are slight differences. These minor differences are caused by finite-size effects (see fig. 3.6). Therefore, the results confirm the validity of eq. (3.3) also for the ASEP in two dimensions. Moreover, the current in the x-direction is apparently not affected by the current in the y-direction despite the simultaneously applied bias $V = F = 1$.

Due to the identical current-density relation of the ASEP in one and two dimensions, it is to be expected that the phase diagram of the one-dimensional ASEP is also valid for the two-dimensional ASEP, which means that there is a first-order phase transition at the coexistence line $\alpha = \beta \leq 0.5$ and a second-order phase transition along the lines $\{\beta > 0.5|\alpha = 0.5\}$ and $\{\alpha > 0.5|\beta = 0.5\}$. This has been verified by checking at distinctive parameter points if the density profiles are consistent with the predictions by the extremal-current principle. The result of the phase diagram and the checked phase transition points are shown in fig. 3.7. Exemplary density profiles for particular α and β are shown in figs. 3.8 and 3.9. In fig. 3.8, where the density has been spatially averaged over the x-th column, one can clearly see that the bulk density corresponds to the set reservoir density ρ_l for the parameter points in the LD-phase and on the coexistence-line. Analogously, this applies for the set reservoir density ρ_r. For the parameter point in the MC-phase, the bulk density is approximately 0.5. In the three-dimensional density profiles, where the density at each site has been measured, the density does not show any significant differences in the y-direction except for the parameter point on the coexistence-line. There is a small dent in the center of the shock front indicating that the shock front is not stationary.

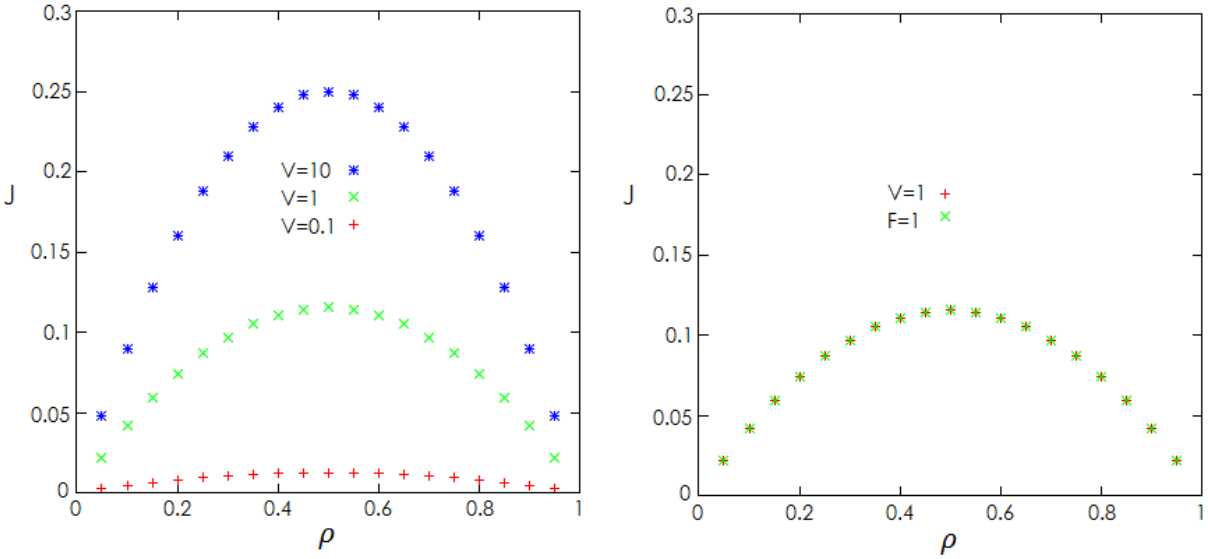

Figure 3.5: Current-density relations of the current in x-direction (left) and additionally in y-direction (right) for different potential strengths V (left) and for a specific potential strength F (right) measured in a system of size [1000×30]. The averaging time has been set to 10^6 time units (corresponding to $10^5 - 10^6$ MCS).

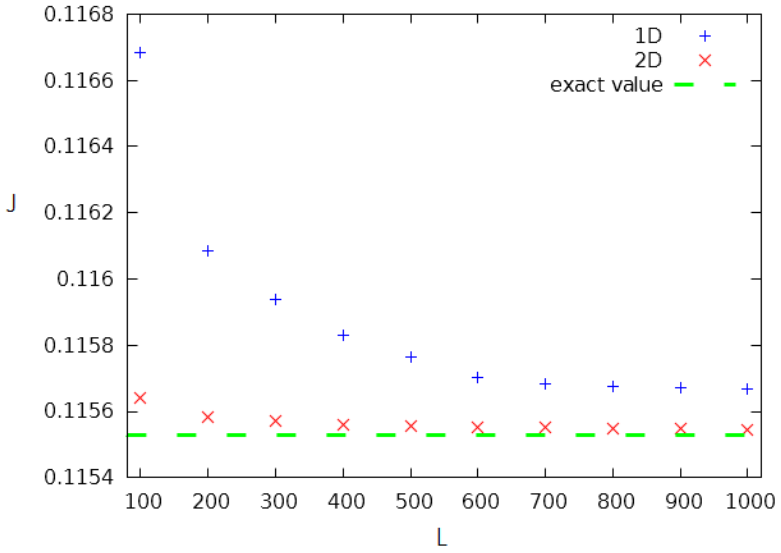

Figure 3.6: Current in systems of width $W = 1$ and $W = 10$, with density $\rho = 0.5$ and potential strength $V = 1$ for different lengths L. The averages were taken over $9{\cdot}10^6$ time units. The finite-size effect causes the difference between measured values and the exact value which is given by eq. (3.3).

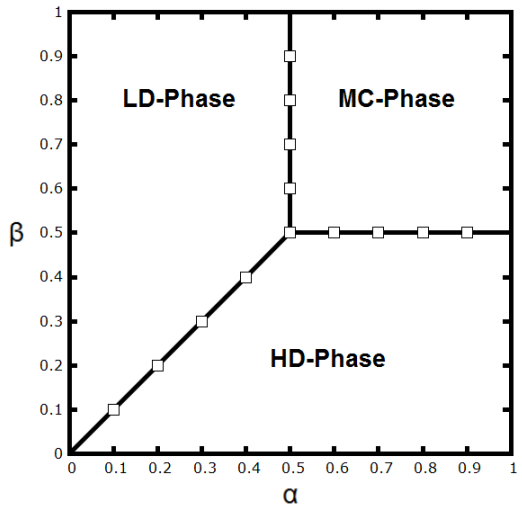

Figure 3.7: Phase diagram of the two-dimensional ASEP. The phase diagrams of the one- and two-dimensional ASEP are identical. At the phase transition points, which are marked by a box symbol, the density profile has been measured. A system size of size [1000×30], a potential strength of $V = 1$ and an averaging time of $0.5{\cdot}10^6$ for the parameter points at the CE-line and $2{\cdot}10^6$ for the parameter points at the boundary to the MC-phase have been chosen.

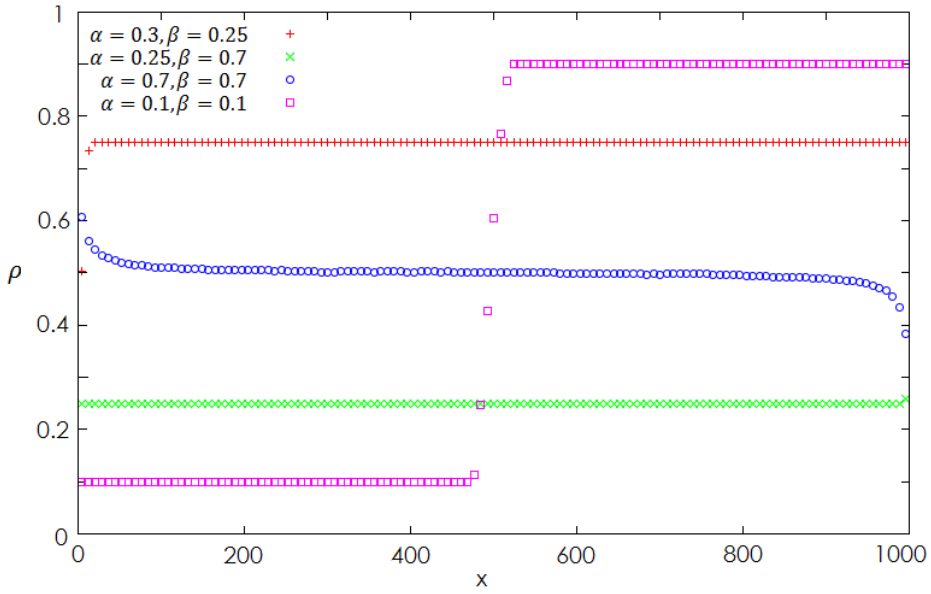

Figure 3.8: Density profiles simulated at four parameter points each representing a different phase except for the last. Parameters α and β are specified in the legend, while the other parameters are the same as in fig. 3.6.

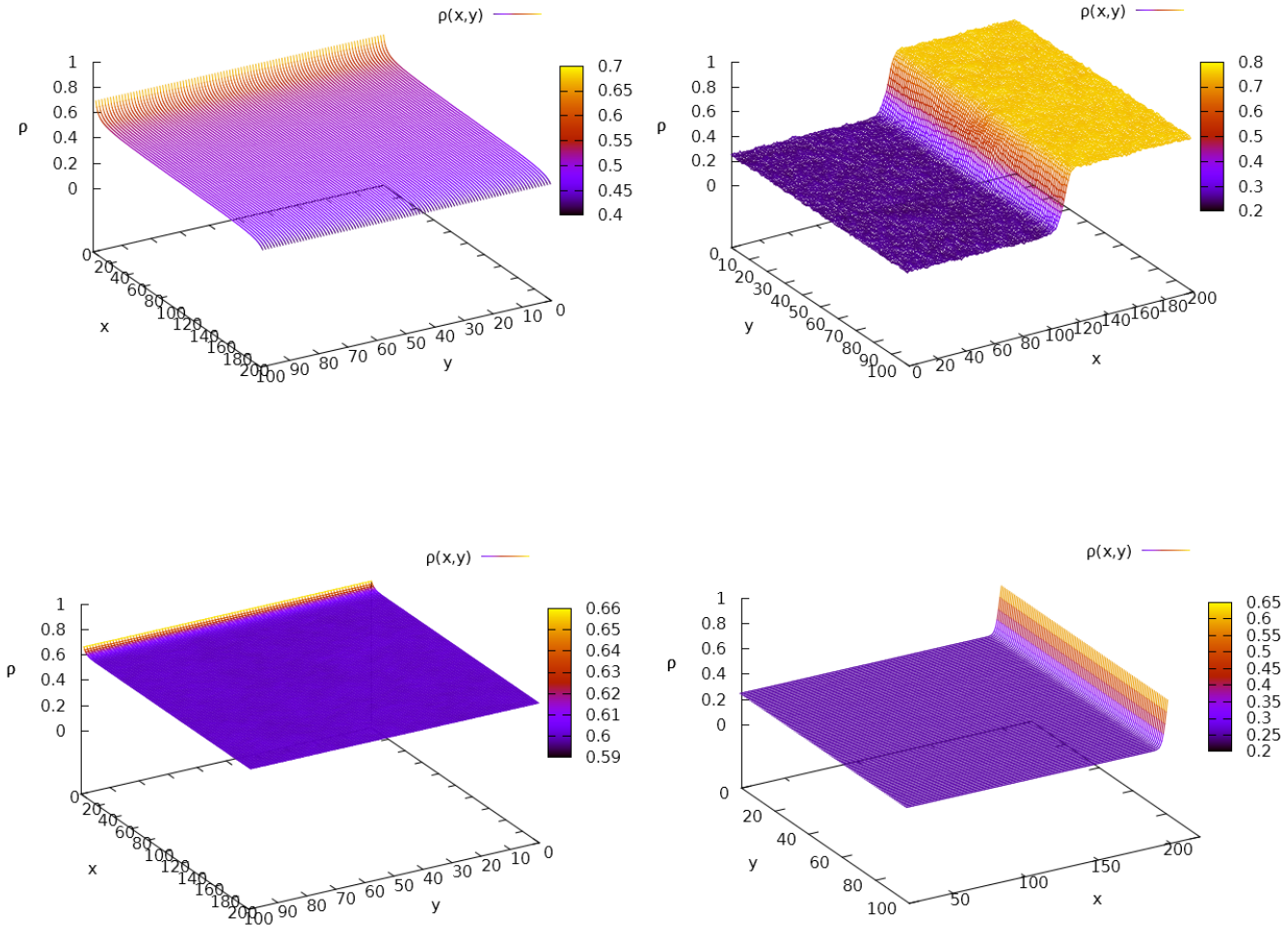

Figure 3.9: Density profiles at the parameter points $\alpha = 0.8$, $\beta = 0.6$ (top left), $\alpha = \beta = 0.25$ (top right), $\alpha = 0.7$, $\beta = 0.4$ (bottom left) and $\alpha = 0.25$, $\beta = 0.3$ (bottom right) were taken over an averaging time of $4{\cdot}10^6$ time units at all parameter points except for the one on the CE-line. Here, the density has been averaged only over $8{\cdot}10^3$ time units to show fluctuations in the shock front. The potential strength was $V = 5$. For a better presentation of the density profile, the coordinate axes x and y were interchanged on the right side.

3.3 Analysis of the Shock Profile

In the previous chapter has been ascertained, that the phase diagram and the current-density relation of the two-dimensional ASEP are consistent with the results in one dimension. In this chapter, a specific phenomenon in the ASEP will be more closely examined with regard to the dependence on the second dimension. This phenomenon is the fluctuating shock front occurring at parameter points on the coexistence line. Shock fronts have already been extensively studied in ref. [ACJL92] by F. J. Alexander *et al.*, though in their ASEP-model, the origination of the shock is different. In their model, it emerges as a result of the introduction of a blockage at a strip of width W between the last and the first column in a bulk system. The transition between these columns is suppressed by a factor $0 \leq r \leq 1$, where $r = 0$ equals a total inhibition and $r = 1$ no perturbation. Thus, the model studied by F. J. Alexander *et al.* consists of a perturbed bulk system and the shock front is rather artificial in contrast to the inherent shock in the open system. Moreover, in the open system the shock-front separates two phases of particular densities specified by the reservoir densities. In the bulk system, the entire density profile changes, when the shock front moves, since the number of particles is conserved. Because of these differences, the two models are in general not comparable. The purpose of their investigation of the shock fluctuation has been the study of the scaling behaviour of microscopic fluctuations in the context of growth models, which have been intensively discussed at that time [KPZ86]. The shock front represents in this case the growing interface.
A theoretical approach to describe the growth of interfaces has been proposed by M. Kardar, G. Parisi and Y. C. Zhang. From considerations of a coarse grained interface, the Kardar-Parisi-Zhang (KPZ) equation has been derived [KPZ86]:

$$\frac{\partial h}{\partial t} = v_0 + \nu \Delta h + \frac{\lambda}{2}(\nabla h)^2 + \eta(\vec{x},t), \tag{3.19}$$

where $h(\vec{x},t)$ represents the local 'height' of the interface, ν and λ are physical constants, which are related to the surface tension and the growth velocity respectively, and η is a Gaussian-distributed noise with $\langle \eta(\vec{x},t)\eta(\vec{x}^*,t^*)\rangle = 2D\delta^d(\vec{x}-\vec{x}^*)\delta^d(t-t^*)$.
By choosing a moving coordinate system, the time-independent growth velocity constant v_0 can be omitted. The second term on the right side of the equation describes the lateral relaxation. By the third term is considered that an inclination implies a non-linearity in the growth rate. The noise covers the aspect of randomness of the growth rate and can be modified to adapt it to the model, which is studied. The KPZ-equation can be mapped onto the Burgers equation with the transformation $u = -\nabla h$, which can be interpreted as a model for a vorticity-free velocity field [KPZ86]. It is one of the simplest models exhibiting shock waves as a solution. These shock waves travel with a deterministic velocity. In the ASEP, however, neither the shock front occurring at the coexistence line nor the shock front discussed in ref. [ACJL92] are showing a constant drift. In ref. [ACJL92], it has been argued that the shock front is described by the linearized KPZ-equation, alias the Edward-Wilkinson (EW) equation, which can be readily solved using Fourier-transformation. In the conclusion, the theoretical predictions by the solution of the linearized KPZ-equation for the scaling behaviour of various quantities have been compared to the numerically obtained results.
Here, a similar analysis has been conducted but on a smaller scale and for the open system.

3.3.1 Identification of the Shock

In the open system, the shock front appears as the border separating the LD-region from the HD-region with densities ρ_l and $1-\rho_l$ respectively. Since the ASEP describes a discrete

system (particles on a lattice with hard-core repulsion interaction), the identification of the shock poses a problem. Two methods have been used to determine the position of the shock.
The first method is the direct and straight-forward option. Here, the density profile is measured for short time intervals. The choice of the time interval, alias windowing, is not a trivial issue, since longer intervals allow more accurate density profiles, but also involve an averaging over more shock positions which leads to a broader shock front. On the other hand, if the time interval is chosen too short, density fluctuations may lead to a flawed detection of the shock position. For these reasons, the choice of the time interval is a compromise between detection accuracy and a small time window.
The second method is related to the mentioned second-class particles in ch. 3.1.2. It has been proved that second-class particles are driven to the shock [Fer92] and therefore, they offer a rather uncomplicated identification of the shock position. Still, the introduction of second-class particles increases the complexity of the dynamics and in two dimensions the vertical movement complicates the determination of the position of the shock.
A much simpler approach, proposed in ref. [ACJL92], consists of the introduction of so-called 'shadow particles', which do not interact with the system but move in a 'potential', driving the shadow particle into the minimum at the shock position. A better name for these particles may be ghost particles as it provides a better illustration of these particles, which can 'see' and move but not interact. The dynamics of the shadow particles is governed by the following update rule for the position:

$$x_y(t+\delta t) = \begin{cases} x_y(t) - (2n_{xy}(t) - 1) & \text{with a probability } p \\ x_y(t) & \text{with a probability } 1-p \end{cases}$$

Here, x_y represents the x-coordinate of the shadow particle's position in the y-th row and n_{xy} the occupation number of site (x,y). This means that a shadow particle jumps with a probability p to the left, if its current site is occupied, or to the right, if its current site is unoccupied, and stays with a probability $1-p$. A jump in the vertical direction is unprovided for. The shadow particles' positions do not need to be updated after each iteration. Since the shock front is a collective effect, the shock front moves in average after L/W steps.
To identify the position of the shock using the first method, a time interval of about 10 MCS has been chosen. The shadow particles' positions have been updated every half MCS. Additionally, in the first method the density has been averaged over columns, reducing the identification of the shock's position to a one-dimensional problem. Here, a central moving average of the density over 9 sites has been used to identify the position of the shock. If the average exceeds a density of $\rho = 0.5$, the position is found at the center. In the second method, only the last positions of the shadow particles have been averaged. Both methods have been compared in systems with sizes [160×1], [160×3] and [160×9]. As a measure for the correlation between the positions obtained from the different methods, the Pearson correlation has been chosen. It is defined as

$$\rho(X,Y) = \mathrm{cov}(X,Y)/\sigma_X\sigma_Y$$

In the one-dimensional system, it yields a value of ca. 0.99, whereas in the two-dimensional systems the Pearson-correlation yields an average value around 0.999. This difference has been expected because the first method is noticeably more affected by density fluctuations in one dimension than in two dimensions, where beforehand the density has been averaged over columns.

3.3.2 Results of the Scaling Behaviour

As said above, many growth models are described by the KPZ-equation, which means in technical terms, that they lie in the KPZ universality class. Models of this class share a common scaling for the following quantity [ACJL92]:

$$w(W,t) = \Big(\frac{1}{W}\int_W (h(x,t) - \bar{h}(t))^2 dx\Big)^{1/2} \tag{3.20}$$

where W represents the width of the system, which is perpendicular to the growth direction, $h(x,t)$ represents the height at position x and time t and the spatially averaged height at time t is denoted by $\bar{h}(t)$.
In general, w is interpreted as the shock width in growth direction and is described by

$$w \approx W^{\alpha} f(t/W^{\alpha/\beta}) \tag{3.21}$$

with

$$f(t/W^{\alpha/\beta}) \sim \begin{cases} \text{constant} & \text{for } t \gg W^{\alpha/\beta} \\ t^{\beta} & \text{for } t \ll W^{\alpha/\beta} \end{cases}$$

Therefore, the scaling exponents of w are described by the parameters α and β (not to be confused with the parameters in the injection and ejection rate). In the case of the EW-equation, these exponents can be calculated in means of a simple scaling analysis. In two-dimensional systems, they are given by $\alpha = 1/2$ and $\beta = 1/4$ [Fam90].
To test the scaling exponent α, two quantities have been calculated, which show, according to ref. [ACJL92], the same asymptotic scaling. These are the shock width

$$\langle w^2(W)\rangle = \Big\langle \frac{1}{W}\sum_{y=1}^{W} (h(y,t) - \bar{h}(t))^2 \Big\rangle_t \tag{3.22}$$

and the truncated height-height correlation function for the m-th neighbour with $m = 1$

$$G(m) = \Big\langle \frac{1}{W}\sum_{y=1}^{W} h(y,t)h(y+m,t) - \bar{h}^2(t) \Big\rangle_t, \tag{3.23}$$

where W is the width of the system, $h(y,t)$ the position of the shock front represented by the position of the shadow particle in the y-th row at time t, $\bar{h}(t)$ the mean height at time t and $\langle..\rangle$ denotes an average over time.
The results are shown in fig. 3.10. The scaling exponents of w^2 and $G(1)$ do seem to approach the predicted value of $2\alpha = 1$. At least the findings shown in fig. 3.10 are very similar to the findings in ref. [ACJL92], where they concluded that their results also only indicate that the asymptotic scaling exponents are given by α (and β). But this shows that, although the formation of the shock front in the open system is very different to the formation in the perturbed bulk system, the nature of the shock fronts are presumably alike.
Another characteristic of the shock front, which depends on the width and has been studied, is the mean-squared displacement of the position of the shock. It is expected that the MSD increases linear in time (cf. eq. (1.1)) until the limitation by the finite size of the system leads to a saturation of the MSD. The diffusion coefficient D, however, is conjectured to decrease as $1/W$ with increasing width of the system.

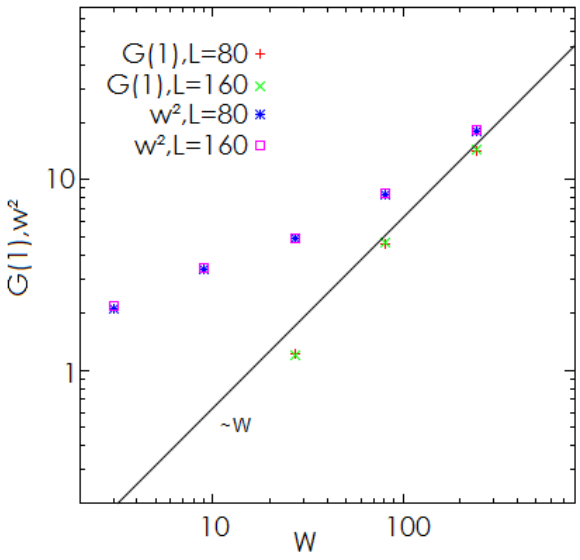

Figure 3.10: The quantities $G(1)$ and w^2 have been obtained from averages over 150000 different configurations of shadow particles in a single run for different widths W. As system parameters has been chosen $\alpha = \beta = 0.25$, $L = 80$ and $V = 5$. Here, the system has been initialized by filling one side of the system with an average density of $\rho_{\text{left}} = 0.25$ and the other side with an average density of $\rho_{\text{right}} = 0.75$ introducing an initially 'sharp' shock front. The initial position of each shadow particle is in the middle of the system. For widths $W < 27$, values of $G(1)$ are negative, which is why they are not shown.

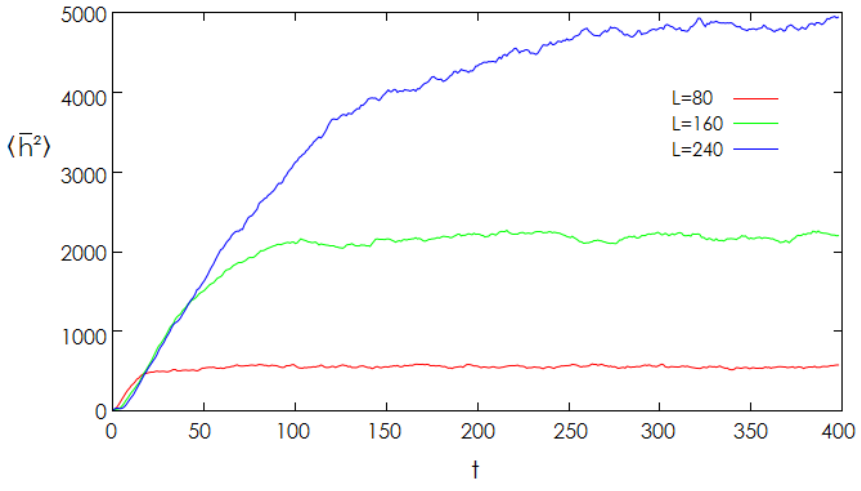

Figure 3.11: Typical behaviour of the MSD of random walkers in finite systems, which is here represented by the shock front. The averages have been taken over 1000 independent runs with the system parameters $\alpha = \beta = 0.25$, $W = 1$ and $V = 5$. The shock position has been identified by using the second method. For widths $W > 1$, a similar behaviour of the MSD has been observed.

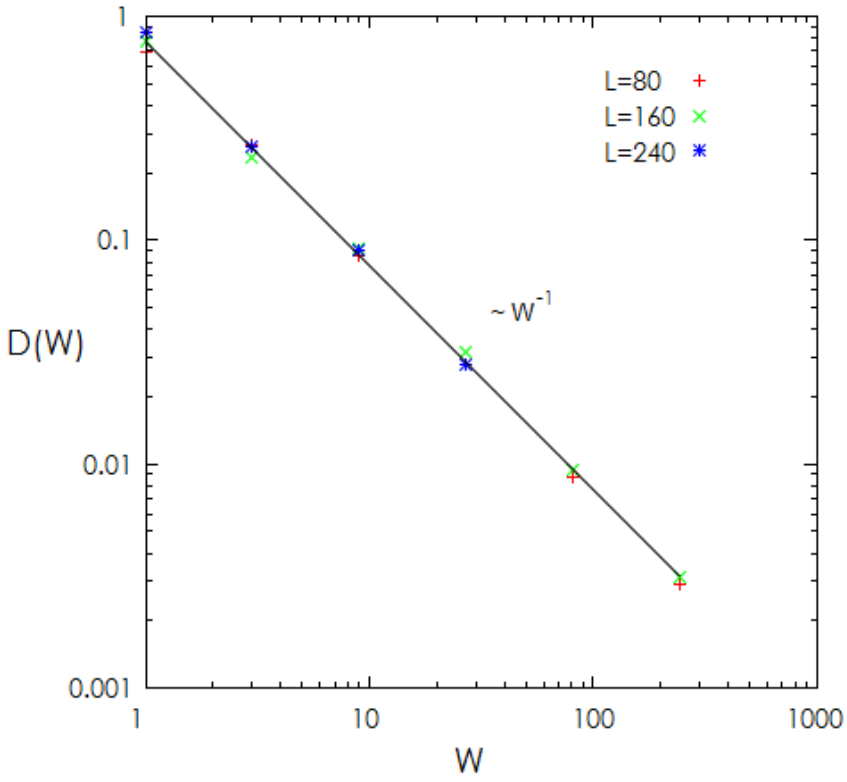

Figure 3.12: As can be seen in fig. 3.11, the MSD increases linearly for a short time interval at the beginning. The diffusion coefficients D for each width W and different lengths L have been obtained by interpolating a segment of the MSD, which lies within this time interval. Therefore, D is represented by the interpolated slope of the MSD.

The typical behaviour of the MSD of the shock position in time is shown exemplarily for width $W = 1$ and different lengths L in fig. 3.11. The result of the dependency of the diffusion coefficient D on the system width W is shown in fig. 3.12. One can see that the results are consistent with the expectation. The reason that the mentioned scaling has been expected is the following: Since the shock front is a collective mode, to change the lateral position of the shock front, the heights $h(y,t)$ in all rows need to be changed in the same direction. Because of this, the movement of the shock front is slowed down by each additional row since the shock position is the average over W positions of shadow particles. To illustrate this behaviour, one could compare the shock of the system with a bulk of particles which is randomly hit by ambient particles. If more particles are added to the bulk, the inertia increases, so that the random fluctuation of the bulk caused by particles in its environment decreases. In respect of this analogy, the cause for this scaling behaviour is rather simple.

4 Brownian Motor

The working principle of Brownian motors has been exemplified by the flashing ratchet. Due to the simplicity of this model, the existence and direction of a non-zero current can be intuitively guessed. But in general, this is not possible as in more complex models e.g. current-reversals can occur upon the variation of certain control parameters. To illustrate the diversity and the extent of complexity of Brownian motors, in the first part of this chapter a brief overview will be given. In the second part, the flashing ratchet model, which has been studied in this thesis, will be discussed.

4.1 Brief Overview of Brownian Motors

In the introduction, a short description of Brownian Motors has been given. A more precise formulation of the hallmarks has been proposed by P. Hänggi *et al*. in ref. [HMN05]. These defining features are [HMN05]:

1. "Spatial and/or temporal periodicity critically affect rectification."
2. "All acting forces and gradients must vanish after averaging over space, time, and statistical ensembles."
3. "Random forces (of thermal, non-thermal, or even deterministic origin) assume a prominent role."
4. "Detailed balance symmetry must be broken by moving the system away from thermal equilibrium."
5. "A symmetry-breaking must apply."
6. State variables are loosely coupled.

Genuine and ingenuine Brownian motors are discerned by the third feature. In genuine Brownian motor models, random forces play a key role, whereas in ingenuine Brownian motors random forces are rather obstructive and a rectification of Brownian motion may even take place in the absence of any noise. One example is the 'Brownian pump' discussed in refs. [DDEM14, Rei02]. The potential is basically a travelling sinus curve and therefore, the working principle is analogous to the working principle of an Archimedes' screw. This means that without random forces a non-zero current is maintained.
One can readily ascertain that in the flashing ratchet model, the mentioned hallmarks apply, but there exists a variety of other Brownian Motor models, which also exhibit the characteristics stated above. In most of these models, a ratchet potential is utilised to break spatial symmetry, but also similar but smoother potentials are imaginable. Many Brownian motor models can be classified into two types, which are referred to as 'tilting ratchet' and 'pulsating ratchet'.
In tilting ratchets, the entire potential landscape is tilted alternately to one side and then to the other side. The tilting may occur randomly or periodically with a certain 'strength'. The corresponding models are termed 'fluctuating force ratchet' or 'rocking ratchet' respectively. To implement this tilting, a force may be applied alternately along the ratchet potential [Rei02]. One realization of a rocking ratchet is shown in fig. 4.1 a). This device has been studied to verify theoretical predictions [BHK94] and an application of this device may be the separation of particles by its sizes, since the transport properties are size-dependent. In the set-up depicted in 4.1 a), the particles are pushed through pores by

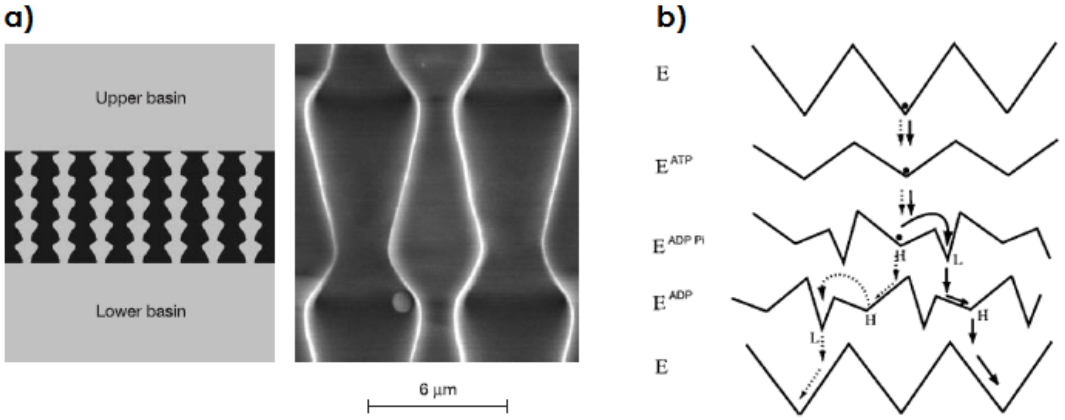

Figure 4.1: Models of Brownian motors: left) a realization of a rocking ratchet [MM03]; right) scheme of an implemented potential modulation to simulate the movement of kinesin proteins [AD99]

applying pressure in the vertical direction. This model is an example, where the current direction reverses, i.e. at a critical pressure amplitude [MM03]. Further discussions of this Brownian motor and rocking ratchets in general can be found in ref. [HMN05] and references therein.
In pulsating ratchets, the potential is varied locally, which is why the flashing ratchet belongs to the 'pulsating ratchet'-type. A model similar to the flashing ratchet is the so-called thermal ratchet. In this model, the temperature increases and decreases periodically. Analogous to the 'on'- and 'off'-phase in the flashing ratchet, the particles are trapped when the temperature is low and when the temperature increases, the influence of the potential lessens. Thus, the effective potential may be described as a rising and falling ratchet potential. The main difference to the flashing ratchet is the continuous variation of the potential instead of an abrupt change [HMN05]. Much more complex dynamics have been assumed in ref. [AD99]. The changes of the potential are shown in fig. 4.1 b). This model has been studied to illuminate an alternative mechanism of locomotion of kinesin proteins. Following their method of changing the potential, one could devise many more models, which can be more complex. Despite the possibilities, mainly only the flashing ratchet has been experimentally studied, due to the simple implementation. Examples can be found in refs. [Rei02, HMN05, HM09, AH02].
Other known types are the so-called 'correlation ratchet' and 'quantum ratchet'. In the correlation ratchet a coloured noise is considered, which induces a rectification even without a potential modulation [HM09]. Quantum ratchets are working in a regime, where quantum mechanical effects have to be taken into account [Rei02].
In conclusion, there exist a variety of different models, which exhibit the characteristics of a Brownian motor.
In the following chapter the flashing ratchet will be discussed. Like in the ASEP, the bulk system and the open system has been studied to investigate the phases in the flashing ratchet.

4.2 Flashing Ratchet

4.2.1 The Model

The flashing ratchet model and the two-dimensional ASEP are modeled very much alike. A discrete square lattice Λ of width W and length L is considered, where particles may move up, down, right and left to an unoccupied site. In this model, the particles also interact only via hard-core repulsion. Similar boundary conditions as in the ASEP can be chosen. Basically, the only difference lies in the change of the potential. Instead of a linearly decreasing potential reflected by a constant bias, a flashing ratchet potential is introduced and an effective bias is caused by the interplay of trapping and free diffusion. The dynamics are therefore ruled by the time constants τ_{on} and τ_{off}, for which the potential is switched on or off, and the form of the ratchet potential, which is characterized by the potential strength $V_{\max}$, the wavelength λ and the position of the potential maximum λ^*, which may be replaced by an asymmetry factor, e.g. $f_{\text{as}} = 1 - \lambda^*/(2\lambda)$, for the purpose of generalization. If the time $\tau_{\text{per}} = \tau_{\text{on}} + \tau_{\text{off}}$ is divided evenly, which means $\tau_{\text{on}} = \tau_{\text{off}}$, for convenience the time parameter $\tau := \tau_{\text{per}}$ is introduced. In the one-dimensional case, pictured in fig. 4.2, the potential $V(x,t) = V(x + n\lambda, t + m\tau_{\text{per}})$ is defined as

$$V(x,t) = \begin{cases} 0 & t \in [0,\tau_{\text{off}}) \ , \ \forall x \\ V_{\max}\lambda^{-1}x & t \in [\tau_{\text{off}},\tau_{\text{per}}) \ , \ 0 < x \leq \lambda^* \\ V_{\max}(\lambda - \lambda^*)^{-1}(\lambda - x) & t \in [\tau_{\text{off}},\tau_{\text{per}}) \ , \ \lambda^* < x \leq \lambda \end{cases} \tag{4.1}$$

Since the schematic illustration of the dynamics does not include the second dimension, for the continuation of the potential into the second dimension, various shifting patterns of $V(x,t)$ are imaginable e.g. a zigzag pattern or a simple shift by one unit in consecutive rows $V(x,y,t) = V(x + y,0,t)$. To describe the potential in the y-direction, a function $F(x,y,t)$ may be introduced. In the studied model, the potential $V(x,t)$ is simply extended into the second dimension, which means $V(x,y) = V(x)$. Thus, $F(x,y,t)$ is generally set to zero. In the studied model, a further condition has been imposed on the system for all simulations by fixing the wavelength λ and the position of the potential maximum λ^* as illustrated in fig. 4.2, which means that λ comprises ten unit lengths and the potential maximum is found at the fourth site.

The denotations for the transition rates are adopted from the two-dimensional ASEP and since Glauber-rates are employed in this model as well, the transition rates are generally given by:

$$p_{\rightarrow} = (1 + e^{-[V(x,y,t) - V(x+1,y,t)]/k_B T})^{-1} \tag{4.2a}$$

$$q_{\leftarrow} = (1 + e^{-[V(x,y,t) - V(x-1,y,t)]/k_B T})^{-1} \tag{4.2b}$$

$$p_{\downarrow} = (1 + e^{-[F(x,y,t) - F(x,y+1,t)]/k_B T})^{-1} \tag{4.2c}$$

$$q_{\uparrow} = (1 + e^{-[F(x,y,t) - F(x,y-1,t)]/k_B T})^{-1} \tag{4.2d}$$

The dynamics of the bulk system are completely described by the above stated rates. For the open system, four additional rates are required, since the couplings to two reservoirs at the left and right boundary have to be taken into account. In this model, two different couplings have been applied [DEM13].

First, the so-called 'bulk-adapted coupling' will be explained. Bulk-adapted means, that the dynamics in the system are also present in the reservoir but with the condition that the average density is fixed. Therefore, reservoirs represent bulk systems to which the system is coupled. By this choice of open boundary condition, the effective density $\rho^*_{l,r}$ at the

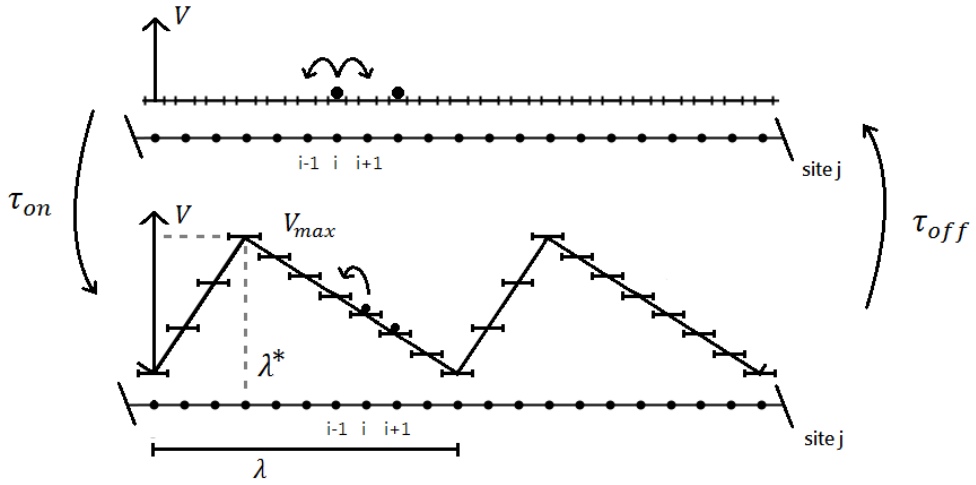

Figure 4.2: Schematic illustration of the dynamics in the flashing ratchet. The control parameters τ_{on}, τ_{off}, λ, λ^* and V_{max} describe the system.

boundary can be directly controlled [DEM13]. Take, for instance, the ASEP model, where the system is coupled to the reservoirs by α and β. The rates in eqs. (3.17) consist of the parameters α or β and the rates to jump to the left or to the right, which is controlled by the imposed bias. In the ASEP, one associates α with the density at the left boundary and $1-\beta$ with the density at the right boundary. The validity of this association is supported by the fact that the phase diagrams obtained by applying the extremal-current principle and by a purely analytical approach are identical when α is replaced by ρ_l and β by $1-\rho_r$. In the ASEP, bulk-adapted couplings are readily realized but in general, the correlations between occupation numbers at all sites, which are affected by the open boundary condition, have to be studied. For a given density ρ_l (ρ_r), one has to determine the conditional probability

$$p(A|B) = \frac{p(A \cap B)}{p(B)} = \frac{\langle \prod_{i=0}^{N_1} n_i | \prod_{j=N_1+1}^{N_2} n_j \rangle}{\langle \prod_{j}^{N_2} n_j \rangle} \,, \tag{4.3}$$

where i and j represent the relevant sites, $A = \{n_0,...,n_{N_1}\}_{n_i=1,0}$ a particular configuration in the reservoir and $B = \{n_{N_1+1},...,n_{N_2}\}_{n_i=1,0}$ a particular configuration in the system where an injection or ejection is possible. The sign '|' indicates the boundary between the reservoir and the system. To actually derive the conditional probability, one calculates the appropriate correlators for the configurations specified by A and B in the bulk system [DEM13]. In the TASEP, this is very simple. For a given density ρ of the bulk system, the parameters α and β, which define the phase in the open system, are given by

$$\alpha = \frac{p(A \cap B)}{p(B)} = \frac{\langle 1|0 \rangle}{\langle 0 \rangle} = \frac{\langle \rho(1-\rho) \rangle}{\langle 1-\rho \rangle} = \rho \tag{4.4}$$

$$\beta = \frac{p(B \cap A)}{p(B)} = \frac{\langle 1|0 \rangle}{\langle 1 \rangle} = \frac{\langle \rho(1-\rho) \rangle}{\langle \rho \rangle} = 1-\rho \tag{4.5}$$

In the flashing ratchet, the determination and realization of the bulk-adapted couplings are more complicated due to the time-dependent dynamics. Moreover, the correlators are in this model also dependent on the position and thus, reservoirs can only be inserted in the open system at the measured positions. In the studied model, the left reservoir is placed next to a potential minimum and the right reservoir is placed at the potential minimum.

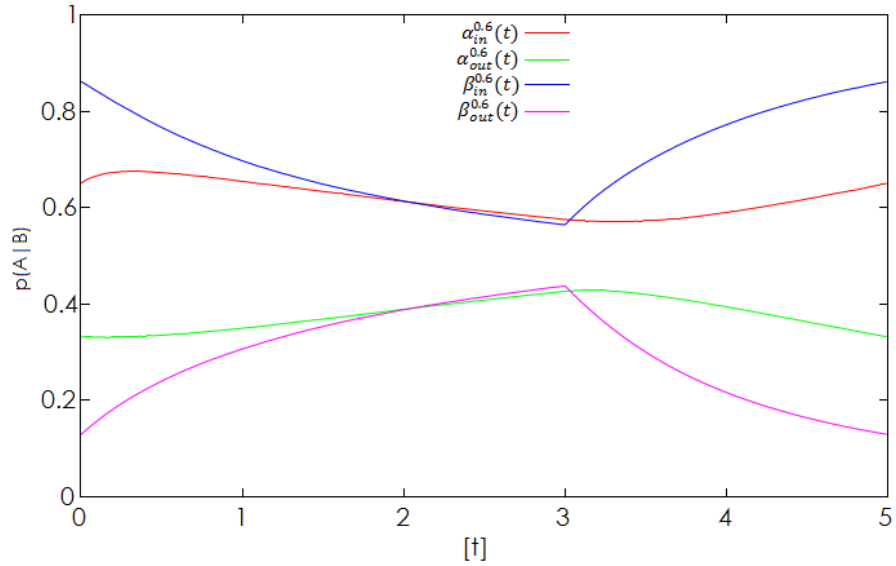

Figure 4.3: The correlators for the parameters $\alpha_{\text{in}}^{0.6}(t)$, $\alpha_{out}^{0.6}(t)$, $\beta_{\text{in}}^{0.6}(t)$ and $\beta_{out}^{0.6}(t)$ given by $\langle 1|0\rangle/\langle 0\rangle$, $\langle 0|1\rangle/\langle 1\rangle$, $\langle 0|1\rangle/\langle 0\rangle$ and $\langle 1|0\rangle/\langle 1\rangle$ respectively are plotted. Due to the time-dependency, the values have been assigned to a time interval of [0.01] centered at a specific time [t]. By [t] is meant the residue class defined as $\{t|t_{time} = n \cdot t_{\text{per}} + t, n \in \mathbb{N}\}$. The averages have been taken over all matching sites in a system of size [150×20] and weighted in a simple manner over a total time corresponding to 10^6 MCS.

Since no exact analytical solution for the discrete flashing ratchet is known, the relevant correlators have been obtained numerically from KMC-simulations of the bulk system for the densities ranging from 0.15 to 0.85 in intervals of 0.05. In fig. 4.3 the findings of the conditional probabilities, which represent the parameters $\alpha_{\text{in}}(t)$, $\alpha_{\text{e}}(t)$, $\beta_{\text{in}}(t)$ and $\beta_{\text{e}}(t)$, are shown for the density $\rho = 0.6$. One can clearly see when the ratchet is switched on or off. As time constants have been chosen $\tau_{\text{on}} = 2$ and $\tau_{\text{off}} = 3$ to see, if differing time constants affect the phase diagram. An effort has been made in identifying the values of these parameters by taking weighted averages.
Due to the time-dependent dynamics, every rate is in general time-dependent. But since in the flashing ratchet only two potential landscapes are considered, which are switched amongst each other after a time τ_{on} or τ_{off}, the rates for transitions within the system are only effectively changing at these instants. The injection and ejection rates for the bulk-adapted couplings are given by

$$\Gamma_{L,in}(t) = \alpha_{\text{in}}(t)(1 + e^{-[V(-1,y,t)-V(0,y,t)]/k_BT})^{-1} \tag{4.6a}$$
$$\Gamma_{L,e}(t) = \alpha_{\text{e}}(t)(1 + e^{-[V(0,y,t)-V(-1,y,t)]/k_BT})^{-1} \tag{4.6b}$$
$$\Gamma_{R,in}(t) = \beta_{\text{in}}(t)(1 + e^{-[V(L+1,y,t)-V(L,y,t)]/k_BT})^{-1} \tag{4.6c}$$
$$\Gamma_{R,e}(t) = \beta_{\text{e}}(t)(1 + e^{-[V(L,y,t)-V(L+1,y,t)]/k_BT})^{-1} \tag{4.6d}$$

Due to the time-dependency of the injection and ejection rates, the advancement in time Δt is obtained by calculating the integral (2.2). There are two possibilities to solve this integral. The first method would consist of fitting a function to the parameters $\alpha_i(t)$ and $\beta_i(t)$. Since a change in a system parameter, that is to say the density ρ, the wavelength λ, the characteristic length λ^*, the potential strength V_{max} or the time parameters τ_{on}

and τ_{off}, leads to a different curve of $\alpha_i(t)$ and $\beta_i(t)$, this method seems rather inefficient. The second method is the numerical integration during KMC-simulations, where no additional care of the form of $\alpha_i(t)$ and $\beta_i(t)$ has been taken. Here, this method has been implemented by using the trapezoidal rule. There are various other methods of computing integrals numerically, which can be found under the keyword Newton-Cotes formulas, but due to the fact, that time steps occur, which are smaller than the distance between two sampling points, this simple method has been chosen. In the simulation, closed expressions have been used to determine if the new time is found before, at or after the next sampling point.
The second type of coupling is called 'equilibrated-bath-coupling'. In this case, the reservoirs are represented by fermionic baths or rather equilibrated Fermi gases. Therefore, the density of the reservoir is given by the average occupation number described by the Fermi-Dirac distribution

$$\rho = \langle n \rangle = (1 + e^{-\mu/k_B T})^{-1} \tag{4.7}$$

where μ corresponds to the chemical potential of the bath. One assumes that the dynamics of the system do not affect the reservoirs due to fast equilibration in the reservoirs [DEM13]. Since in the flashing ratchet all gradients have to vanish when averaged over time and space, particles in the left reservoir have to be on the same energy level as particles in the right reservoir. Therefore, differences between the energy levels in the system and in the reservoirs have to be taken into account in the definition of the injection and ejection rates. This is realized by introducing virtual sites representing the reservoirs, which are on the same energy level. Considering that μ describes the change of energy of a system upon the variation of the number of particles, the injection and ejection rates are given by

$$\Gamma_{L,\text{in}} = \rho_l/(1 + e^{[-(\Delta E)_l - \mu_l]/k_B T}) \tag{4.8a}$$

$$\Gamma_{L,\text{e}} = (1 - \rho_l)/(1 + e^{[+(\Delta E)_l + \mu_l]/k_B T}) \tag{4.8b}$$

$$\Gamma_{R,\text{in}} = \rho_r/(1 + e^{[-(\Delta E)_r - \mu_r]/k_B T}) \tag{4.8c}$$

$$\Gamma_{R,\text{e}} = (1 - \rho_r)/(1 + e^{[+(\Delta E)_r + \mu_r]/k_B T}) \tag{4.8d}$$

where $(\Delta E)_{l,r}$ represents the potential difference between the most left or most right site and the virtual site in the reservoir. The prefactors in eqs. (4.8) imply that the probability to find the virtual site occupied or vacant is controlled by the set density. As the result, equilibrated-bath couplings imposes the set densities on virtual sites, whereas bulk-adapted couplings ensure that the average density of the entire reservoir coincides with the set density. Therefore, this choice of coupling is more realistic due to the absence of dynamics in the reservoir. As will be seen later, the 'rigid' density will greatly affect the phase diagram. The reason is that in the flashing ratchet model, where the ratchet potential is switched on and off, the density averaged over time will be maximal at sites, where the potential is minimal, and minimal at sites, where the potential is maximal, and thus the positioning of the boundaries or the virtual sites is a crucial factor. One may relate the set densities $\rho_{l,r}$ to effective densities $\rho^*_{l,r}$, which correspond to reservoir densities in the open system with bulk-adapted couplings, in order to compare both systems. Like in the ASEP, for convenience, $k_B T$ is set to one.

4.2.2 Investigation of the Flashing Ratchet

In the chapter 3.1.3, it has been presented in detail, how the phase diagram can be derived by the extremal-current principle, if the current-density relation is known. For this reason, first the current-density relation will be discussed. In fig. 4.4, the current-density relations for different potential strengths and different time constants τ_{on} are shown. The difference between the current-density relations, when different time constants are used, is noticeable. Furthermore, one can see in the case of a high potential strength, that the current-density relation resembles the parabolic current-density relation in the ASEP, but the slope at low or high densities appears rather linear. This means that the current is proportional to the density of the particles for low densities and due to the particle-hole symmetry in the flashing ratchet, the current also increases linearly with the density of the holes. The reason for the linear behaviour is the origin of the current in the flashing ratchet. Since the current arises from the dynamics, it is not dependent on the density of holes, if the density of particles is very low. Analogously, this applies to low densities of holes. In simple terms, the current can be understood as the sum of independent one-particle currents. Therefore, eq. (3.3) only applies to density regions, where this simplification of one-particle currents is not correct anymore. Consequently, the current-density relation shows a very similar behaviour as in the ASEP but a variation of the slope of the curve is clearly visible, which means that the current is probably not described by a simple expression as in the ASEP. Since the slight differences only result in small shifts of the current-density dependency and critical properties of the current-density relation are not affected, the derivation of the phase diagram by the extremal-current principle is not different to the discussion in ch. 3.1.3. This means that the phase diagram of the flashing ratchet does not differ from the phase diagram of the ASEP when bulk-adapted couplings are applied. This has been verified by measuring the density profile at distinctive parameter points in the open system, which are shown in figs. 4.5 and 4.6 (left side). One can clearly see, that the behaviour of the moving average of the density is similar to the density profiles shown in fig. 3.8, which means that the flashing ratchet model has similarities with the ASEP, but due to the the ratchet potential, the width of the domain wall is greater than in the ASEP.

For low potential strengths, the current nearly vanishes and shows an asymmetrical behaviour. Current fluctuations is probably the cause of this asymmetric current-density relation, as the effects of the ratchet potential are nearly disappearing and the model approaches an equilibrium system without a ratchet potential. Thus, one might not find definite phases in the density profile from an open system because the system is basically governed by the diffusion current.

Here, it has been found that the phase diagrams of the ASEP and of the flashing ratchet are identical if bulk-adapted couplings are used. The other type of coupling, which has been introduced, is the equilibrated-bath coupling. To determine the phase diagram, when equilibrated-bath coupling are utilised, the density profiles at various parameter points have been measured. To show that the phase diagrams are not the same, the density profiles at the same parameter points have been measured (see. figs. 4.5 and 4.6 (right side)).

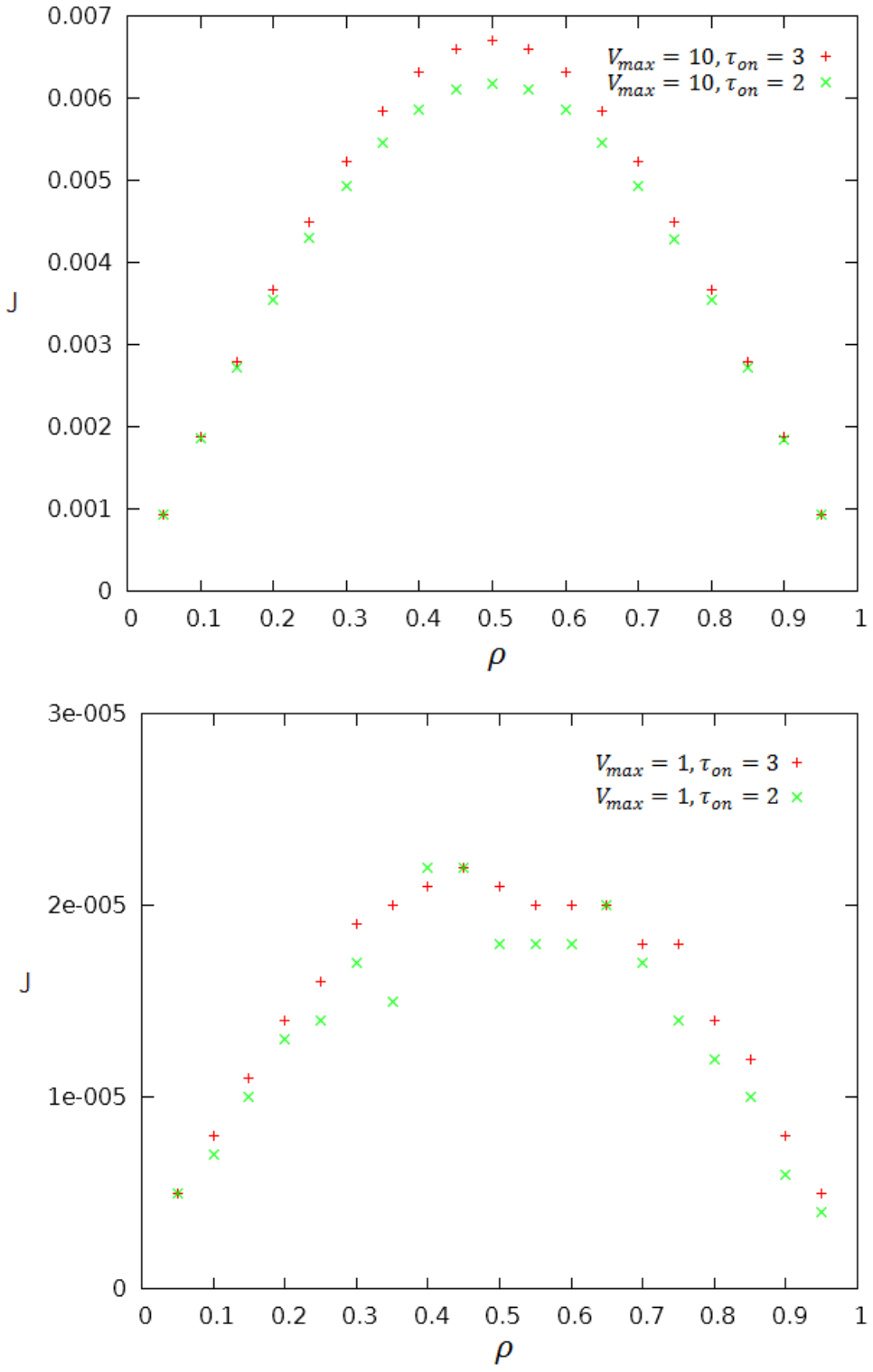

Figure 4.4: Current density relation for the current in the x-direction for different potential strengths $V_{\max}$ and for different time constants τ_{on} measured in a system of size [1000×30] and averaged over a time of 10^6 time units, which corresponds to more than 10^5 MCS. The time constant τ_{off} has been chosen as $\tau_{\text{off}} = 3$.

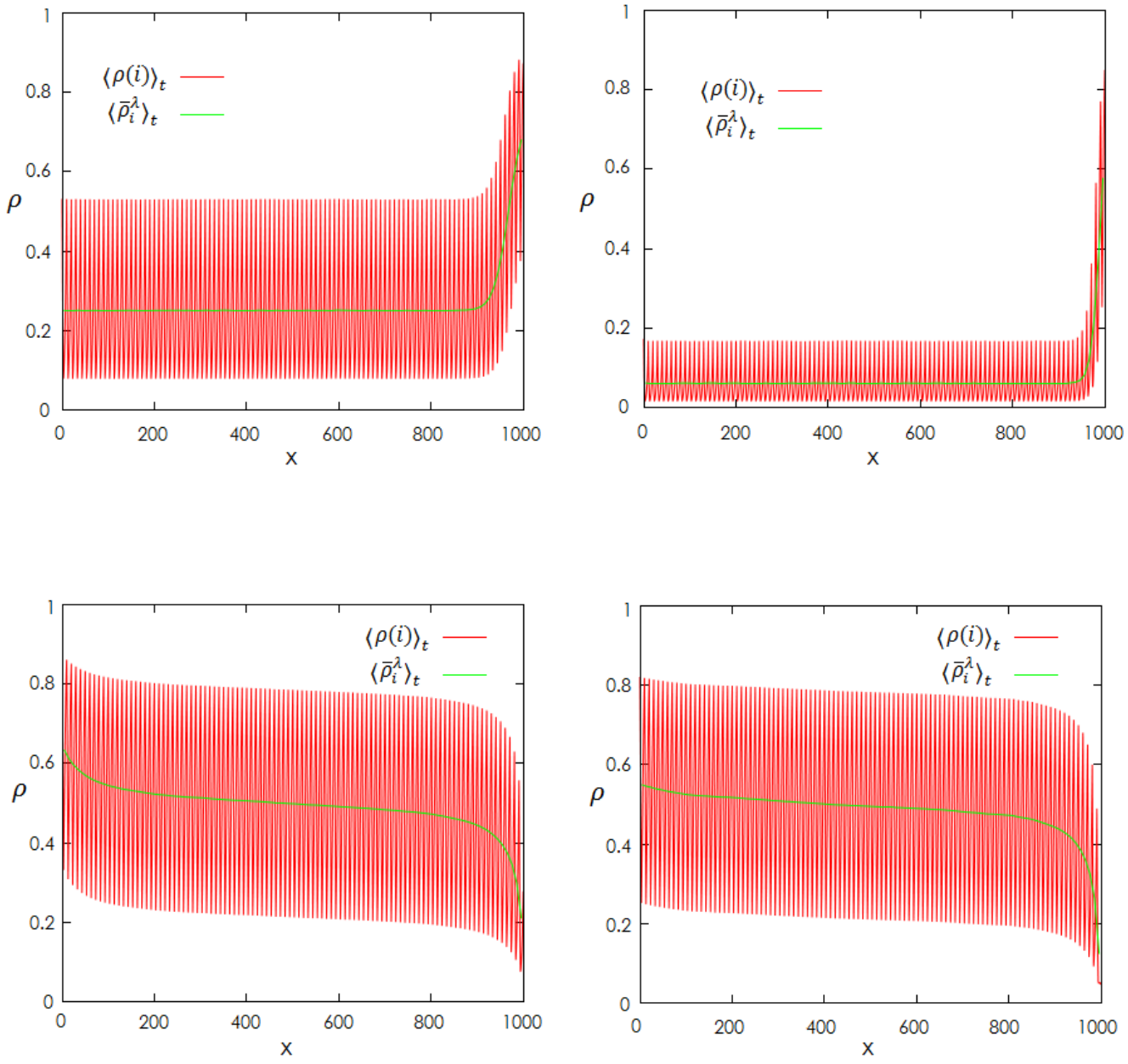

Figure 4.5: Density-profiles for the parameter points $\rho_l = 0.25$, $\rho_r = 0.7$ (top) and $\rho_l = 0.65$, $\rho_r = 0.15$ (bottom) averaged over columns (red) and additionally averaged over the wavelength λ (green) are shown. At the left side, bulk-adapted couplings have been used, whereas on the right side equilibrated-bath couplings have been applied. The size of the system is [1000×30], the potential strength is $V_{\max} = 10$ and averages have been taken over $1.5{\cdot}10^6$ time units. As stated above, the time constants are given in all open systems by $\tau_{\text{on}} = 2$ and $\tau_{\text{off}} = 3$.

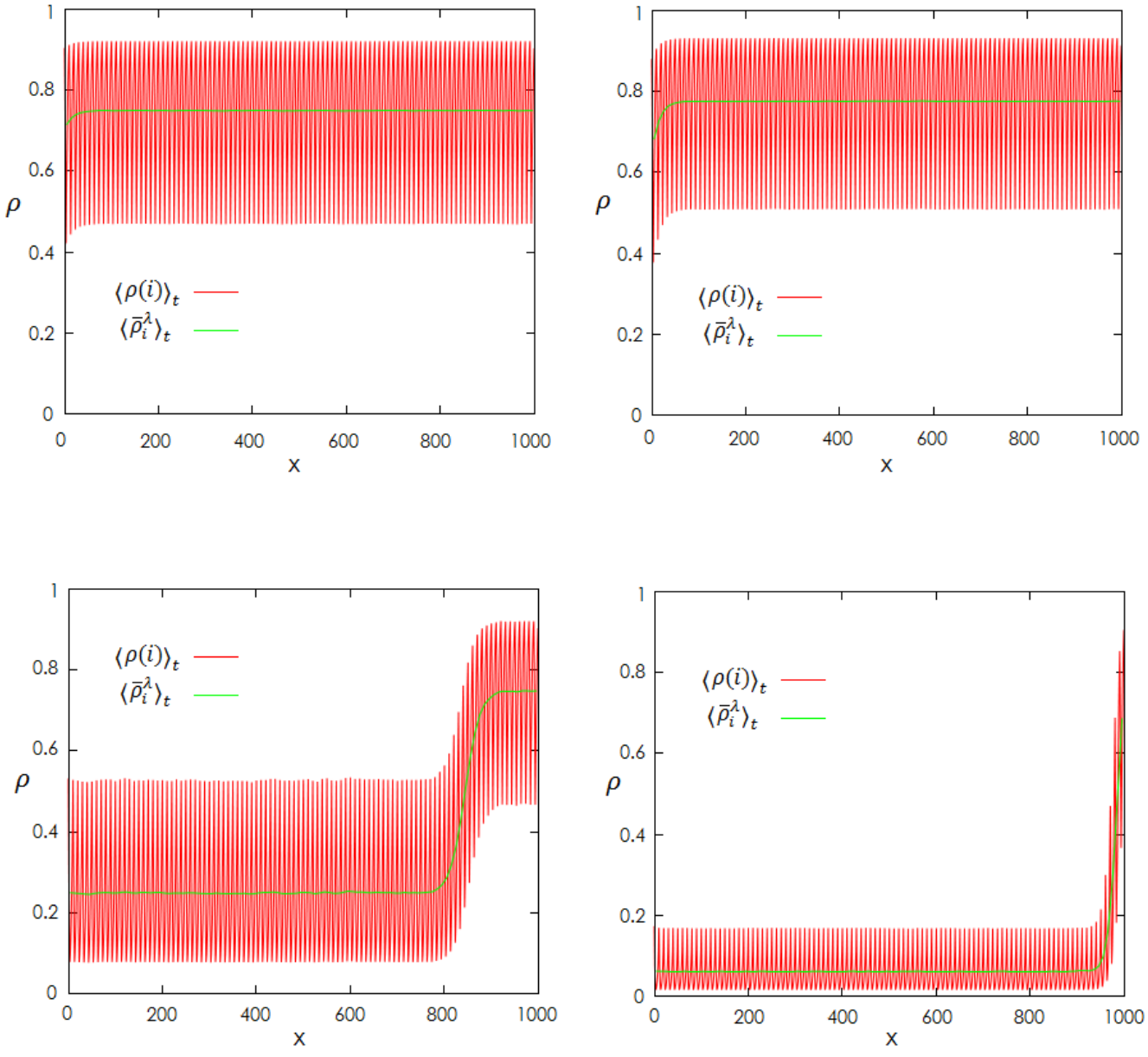

Figure 4.6: Density-profiles as in fig. 4.5 for $\rho_l = 0.7$, $\rho_r = 0.75$ (top) and $\rho_l = 0.25$, $\rho_r = 0.75$ (bottom). For the density-profile at the bottom left, the averaging time was 10^5 time units.

In order to determine the phase diagram of the flashing ratchet model with equilibrated-bath couplings, the boundaries between the MC-phase, the LD-phase and the HD-phase have been located. The first-order phase transition can be readily located. Due to the symmetric current-density relation, the shock front occurring at the CE-line separates the LD-region from the HD-region, where $\rho_l + \rho_r = 1$ holds. Therefore, the density near the left and right reservoir has been investigated. The second-order phase transition is not readily detectable. Because of the parabolic increase of the current, where the maximum indicates the phase boundary to the MC-phase, it is not clearly visible, where exactly the boundary is found. Therefore, the density has been examined because the density profile should show a prominent change. But due to the ratchet potential, differences in the average density are not as evident as in the ASEP, so that an adaption is necessary to discern the difference in the density profile upon the variation of the respective reservoir-density. The bulk-density ρ_b approaches the effective densities ρ_l^* in the LD-phase and ρ_r^* in the HD-phase, thus the moving average is almost constant on the left side of the density profile in the LD-region and on the right side in the HD-region. According to the extremal-current principle, ρ_b is not dependent on the reservoir densities in the MC-phase, since the density, at which the current is maximized, is determined by the current-density relation. As aforementioned, changes in the density profile are not readily visible, but this characteristic change in the density profile after the phase transition will still occur. Thus, one could find the boundary by calculating the derivative of the moving average of the density because in the MC-phase the derivative is negative at both ends. A similar but more direct method has been used here. The density profile has a periodic structure due to the ratchet potential. Therefore, minima (or maxima) are found equidistantly apart and because the minima exhibit a similar behaviour as the moving average, one can simply calculate the following sum, which is approximately zero in the LD- or HD-phase and becomes non-zero in the MC-Phase:

$$\Delta_{LD}^{\min} = \frac{1}{L/2-1} \sum_{i=1}^{L/2-1} \rho_0^{\min} - \rho_i^{\min} \tag{4.9a}$$

$$\Delta_{HD}^{\min} = \frac{1}{L/2-1} \sum_{i=L/2}^{L-2} \rho_{\text{last}}^{\min} - \rho_i^{\min}, \tag{4.9b}$$

where $\rho_i^{\min}$ denotes the density of the i-th minima and L the length of the system.
The results are shown in fig. 4.7. One can see that the boundary between the LD-phase and the MC-phase does not vary along ρ_r. This is expected since in this simple model the maximum-current is given by $\rho_l^* = 0.5$, which is represented only by a specific value of ρ_l. The same applies for the boundary between the LD-phase and the MC-phase. The result for the phase diagram of the open system with equilibrated-bath couplings is shown in fig. 4.8. Additionally, the parameter points, where the effective densities of the reservoirs correspond to the reservoir-densities in the open system with bulk-adapted couplings used in figs. 4.5 and 4.6, have been located. The corresponding density profiles are shown in fig. 4.9 and the different parameter points are indicated in fig. 4.8.

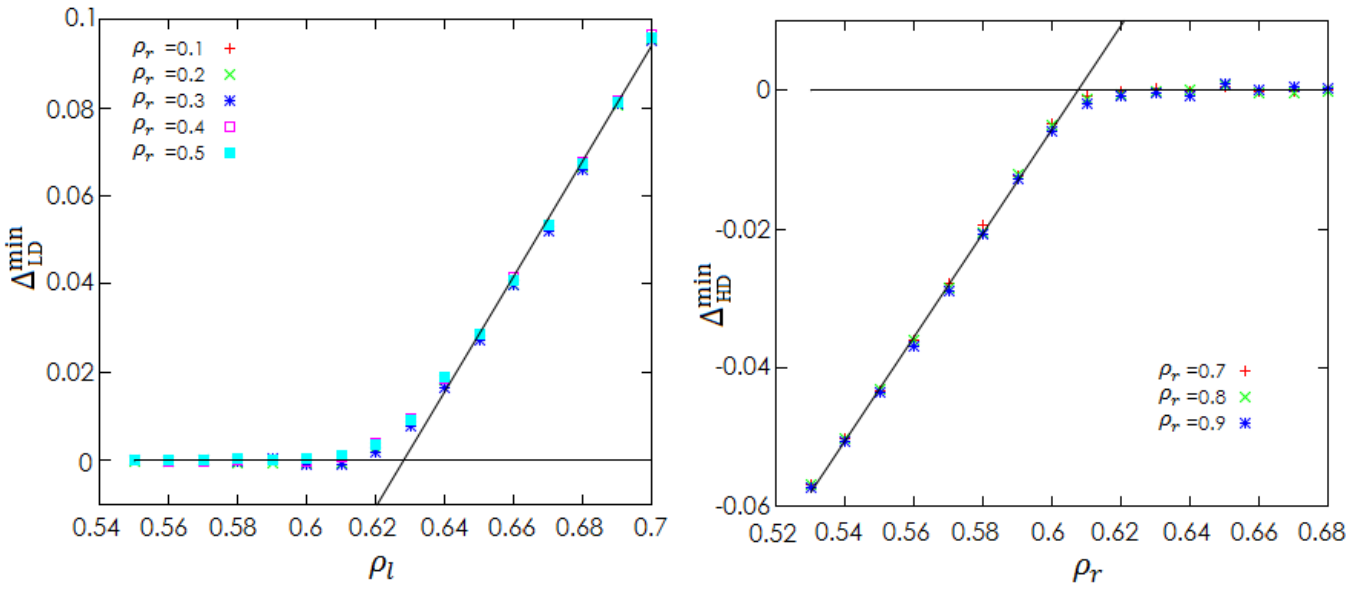

Figure 4.7: The quantities $\Delta^{\min}_{LD}$ and $\Delta^{\min}_{HD}$ have been calculated by taking 50 minima of density profiles into account, which have been obtained as in fig. 4.5. 50 minima correspond to half the system length. The boundaries marking the second-order phase transition were obtained by the depicted interpolation.

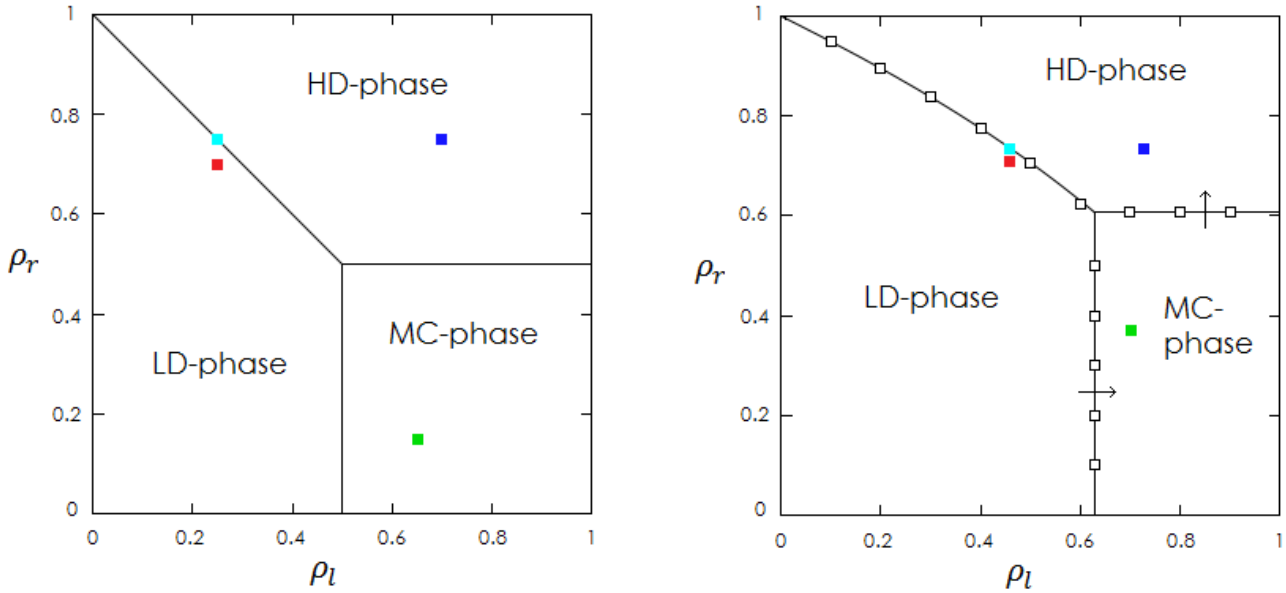

Figure 4.8: Left: Phase diagram of the open system with bulk-adapted couplings; Right: Phase diagram of the open system with equilibrated-bath couplings; tested parameter points are marked by an empty box and lines indicate phase boundaries. The coloured boxes represent the parameter points, where the effective densities of the reservoirs are very similar.

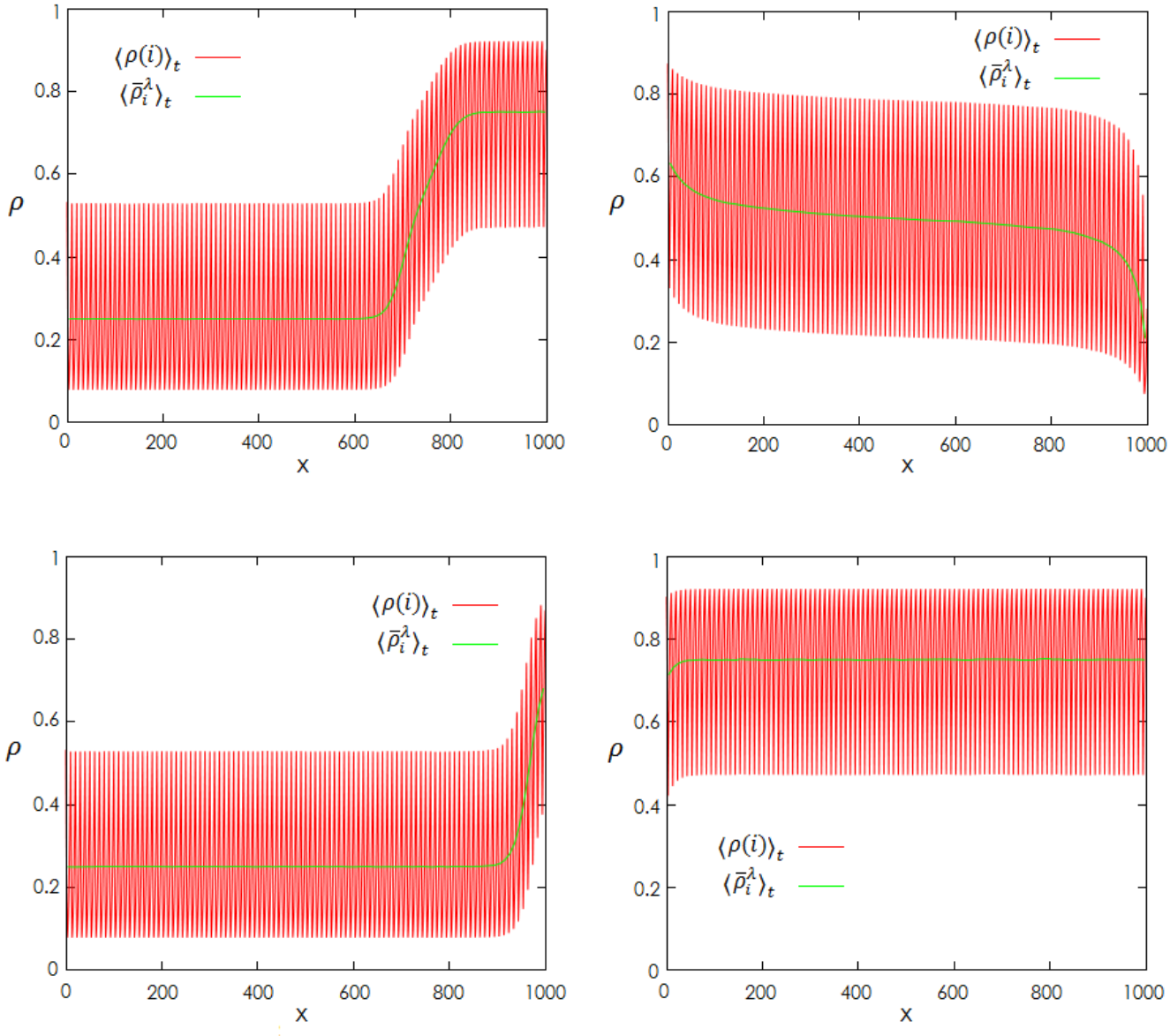

Figure 4.9: Density profiles at parameter points $\rho_l = 0.459$, $\rho_r = 0.7357$ (top left), $\rho_l = 0.7015$, $\rho_r = 0.37$ (top right), $\rho_l = 0.459$, $\rho_r = 0.7075$ (bottom left) and $\rho_l = 0.7277$, $\rho_r = 0.7358$ (bottom right) with the same set of parameters as in fig. 4.5. The density profiles here are similar to the density profiles of the open system with bulk-adapted couplings shown in figs. 4.5 and 4.6.

4.2.3 Parameter Optimization

The flashing ratchet is an example for a Brownian motor and like for all motors the efficiency and the performance are important factors in applications. Therefore, a qualitative analysis of the dependency of the current on control parameters will be conducted. As a simplification, a bulk system of size [800×20] with an average density of $\rho = 0.5$ is considered. The time constant τ_{on} is set equal to τ_{off}.
The 'performance' is in this model represented by the current $\langle J \rangle$ and the dependency of the current on the switching frequency of the ratchet potential $f = 1/\tau$ and on the potential strength $V_{\max} =: V$ has been tested. In multiple studies concerning the efficiency of Brownian motors, an additional work load has been implemented in the system, so that the performance has the correct dimension and the efficiency becomes dimensionless (see ref. [HM09] and references therein). In this qualitative analysis, no workload is applied and thus, the 'efficiency' will be here defined as the ratio of the current to the average power input at one site of the system. Hence, it is given by $fV/2$. Although work is only done, when the energy level of a particle is lifted by the ratchet potential, the above stated expression for the average power input should result in a similar behaviour of the efficiency.
The result of the 'performance' in dependence of switching frequency and potential strength are shown in fig. 4.10. One can see that the current first increases proportional to f, but then it saturates approximately at the frequency $f = 0.1$. In the inset, a small local maximum is visible. For low potential strengths, the current is also very low and it saturates at high potential strengths. This behaviour has also been observed in the previous subchapter. The initially linear dependency of the current on the frequency is expected because the system can be described in the limiting case by two equilibrium systems, where the initial condition for the particle distribution for one system is given by the particle distribution of the other system. Therefore, the current is proportional to the frequency f. This should apply for every sufficiently high potential strength since current fluctuations are inhibited by high potential strengths. One might expect, that the current also decreases, when τ is of the order of the mean waiting time. But since the working principle is completely different, as the current does not arise anymore from the dynamics, more precisely from the 'trapping' and free diffusion, it is not predictable how exactly the current behaves in very high frequency regions. However, the saturation, which sets in approximately at $f = 0.1$, is due to the limited diffusion time. Because of this, an optimization of the 'performance' regarding the frequency is of limited value, although at least one maximum in the low frequency regime to a fixed potential strength exists.
The behaviour of the 'efficiency' can be derived from the behaviour of the current. In fig. 4.11, one can see that the 'efficiency' is low for high and low potential strengths and also for high frequencies. Since the current saturates at high frequencies, the efficiency decreases. Hence, a flashing ratchet should only be operated in a low frequency regime. The current also saturates at high potential strengths and low potential strengths yield low values for the current. Accordingly, the efficiency is in both cases low as well. In fig. 4.11, the efficiency rises at the lines with $V = 8$ and $V = 16$ significantly with decreasing frequency and eventually saturates. The saturation reflects the regime, where the dependency of the current on the frequency is linear. The slope for higher frequencies is given by $1/f$ since the current is almost constant for high frequencies. An optimal choice for the potential strength might be found between these lines. In general one can conclude, that optimal choices for the frequency lie in the low frequency regime and an adequate potential strength is needed.
Although the best efficiency is given for small frequencies, it is not the best choice in regard to the current, since small frequencies yield small currents. So, the best choice is

found when the product of 'performance' and 'efficiency' is maximal. This is shown in fig. 4.12. One can see that the maximum can approximately be found at a low, but not very low frequency and at an adequate potential strength, as expected.

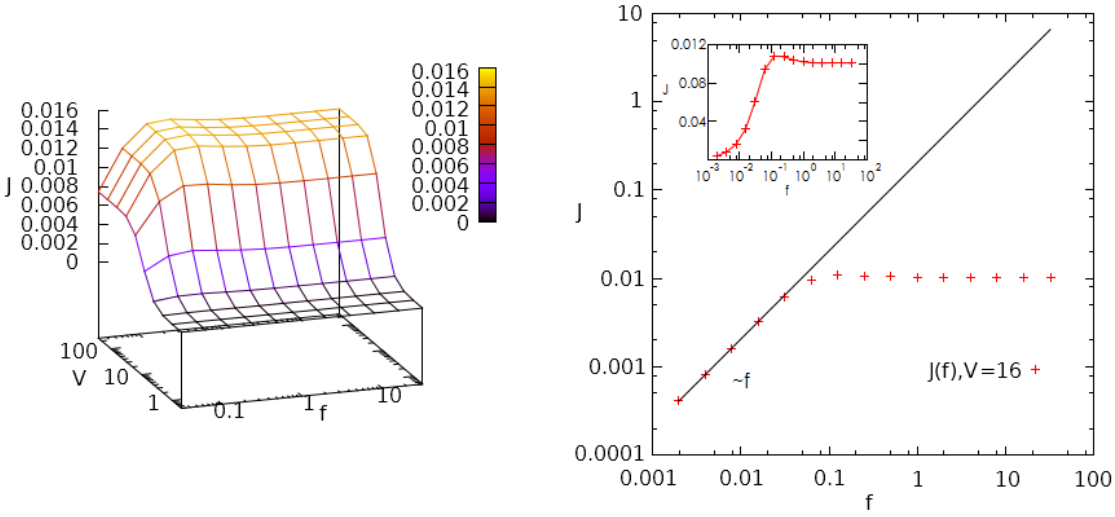

Figure 4.10: On the left side, the current dependent on the parameters f and V is shown. For a wider range of frequencies on the line with $V = 16$, the average current has been examined, which is shown on the right side. In the inset, no logarithmic scale is used for the ordinate. Averages have been taken over 10^6 time units.

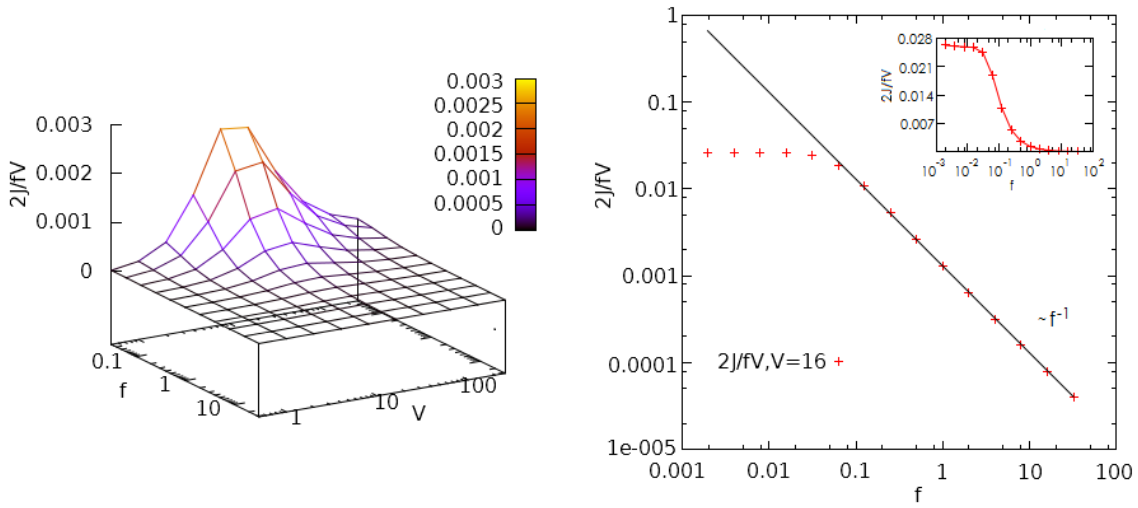

Figure 4.11: The result of the efficiency defined as $2J/fV$ is plotted here. The data of the currents are taken from the results shown in 4.10.

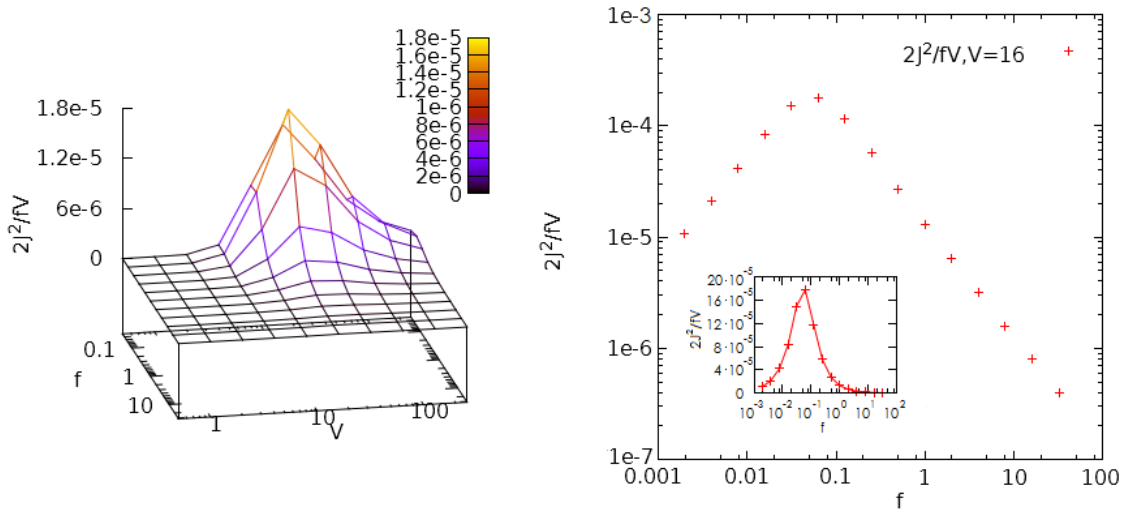

Figure 4.12: In order to find the optimal choice of parameters, which yields a high current and a high efficiency, the quantity $2J^2/fV$ was examined. The result is plotted here.

5 Summary and Outlook

The aim of this thesis has been the study of collective effects and phase transitions of a simple Brownian motor with numerical methods. The model, which has been chosen to represent the simple Brownian motor, is the flashing ratchet. The flashing ratchet is a model for particle transport. Both models have been examined and compared. Since the two-dimensional flashing ratchet has been studied, the ASEP has also been studied in two dimensions in order to enable a better comparability.
The results of this thesis are summarized as follows:

- The ASEP in one dimension has already been studied in-depth. In comparison to the one-dimensional model, the two-dimensional ASEP, which has been examined in this thesis, does not show any significant differences regarding current-density relation or the phase diagram. But it has been shown that the second dimension affects properties of the shock front. In this respect, one may want to keep the method of identifying the shock front by shadow particles in mind, which has been proposed in [ACJL92], since this simple method may also be applicable to other systems.

- In the two-dimensional flashing ratchet, the current-density relation has been measured and the phase diagrams for two different couplings have been investigated and determined. Due to the similar current-density relation of the ASEP and the flashing ratchet, the phase diagram of the open system with bulk-adapted couplings does not differ from the phase diagram of the ASEP. When equilibrated-bath couplings are used, the phase boundaries are shifted and bent since the effective densities of the reservoirs do not coincide with the set densities. But topologically the phase diagram is not different as well. For these reasons, the steady states in the flashing ratchet model are similar to the steady states in the ASEP.

- The flashing ratchet is a Brownian motor and motors are generally characterised by its efficiency and performance. Therefore, the dependency of the current on the switching frequency of the ratchet potential and on the potential strength has been studied. Surprisingly, the current remains constant for a wide range of frequencies and changes mainly upon the variation of the potential strength. In conclusion, it has been found that the best choice of parameters is given by a low frequency and an adequate potential strength.

To sum it up, it has been found that the flashing ratchet model is similar to the ASEP, but instead of a constant bias a net bias occurs as a result from the dynamics. Further issues which still need to be addressed are the behaviour of the shock front in the flashing ratchet and the behaviour of the current for high switching frequencies. In this regard, one may question, if in this case the flashing ratchet can still be considered as a Brownian motor.
Here, the flashing ratchet has only been numerically studied. Due to the similarity of the ASEP with the flashing ratchet it might be possible to derive an analytical solution, at least for the one-dimensional system. But more interesting would be a comparison between experiments and the results found here. For this purpose, the model may probably need to be adapted, so that a reasonable comparison is possible.
Even without comparable experiments, various modifications can be considered. For example, one could study, how shifts in the y-direction of the ratchet potential affects the flashing ratchet or one could introduce additional interactions between particles or include

a second kind of particle which occupies more than one site. The last model may then be comparable to the DNA-oligomers separating device.

References

[ACJL92] F. J. Alexander, Z. Cheng, S. A. Janowsky, and J. L. Lebowitz, *Shock fluctuations in the two-dimensional asymmetric simple exclusion process*, J. Stat. Phys. **68** (1992), no. 5/6, 761–785.

[AD99] R. D. Astumian and I. Derényi, *A chemically reversible brownian motor: application to kinesin and ncd*, Biophys. J **77** (1999), 993–1002.

[AH02] R. D. Astumian and P. Hänggi, *Brownian motors*, Physics Today **55** (2002), no. 11, 33–39.

[AKK+15] M. Aono, S. Kasai, S.-J. Kim, M. Wakabayashi, H. Miwa, and M. Naruse, *Amoeba-inspired nanoarchitectonic computing implemented using electrical Brownian ratchets*, Nanotechnology **26** (2015), no. 23, 234001.

[AP92] A. Ajdari and J. Prost, *Mouvement induit par un potential périodique de basse symétrie: diélectrophorése pulsée*, C. R. Acad. Sci. Paris **315** (1992), 1635–1639.

[BB87] A. L. R. Bug and B. J. Berne, *Shaking-induced transition to a nonequilibrium state*, Phys. Rev. Lett. **59** (1987), no. 8, 948.

[Ber04] H. C. Berg, *E. coli in motion*, Springer-Verlag, New York, 2004.

[BH95] R. Bartussek and P. Hänggi, *Brownsche Motoren*, Phys. Bl **51** (1995), no. 6, 506–507.

[BHH+99] J. S. Bader, R. W. Hammond, S. A. Henck, M. W. Deem, G. A. McDermott, J. M. Bustillo, J. W. Simpson, G. T. Mulhern, and J. M. Rothberg, *DNA transport by a micromachined Brownian ratchet device*, Proc. Natl. Acad. Sci. USA **96** (1999), no. 23, 13165–13169.

[BHK94] R. Bartussek, P. Hänggi, and J. G. Kissner, *Periodically rocked thermal ratchets*, Europhys. Lett. **28** (1994), 459–464.

[BKL75] A. B. Bortz, M. H. Kalos, and J. L. Lebowitz, *A new algorithm for Monte Carlo simulation of Ising spin systems*, Journal of Computational Physics **17** (1975), no. 1, 10–18.

[Bro66] R. Brown, *The miscellaneous botanical works of Robert Brown*, vol. 1, published for the Ray society by R. Hardwicke, London, 1966.

[DDEM14] M. Dierl, W. Dieterich, M. Einax, and P. Maass, *Phase transitions in Brownian pumps*, Phys. Rev. Lett. **112** (2014), 150601.

[DDM92] B. Derrida, E. Domany, and D. Mukamel, *An exact solution of a one-dimensional asymmetric exclusion model with open boundaries*, J. Stat. Phys. **69** (1992), no. 3/4, 667–687.

[DEHP93] B. Derrida, M. R. Evans, V. Hakim, and V. Pasquier, *Exact solution of a 1D asymmetric exclusion model using a matrix formulation*, J. Phys. A: Math. Gen. **26** (1993), 1493–1517.

[DEM13] M. Dierl, M. Einax, and P. Maass, *One-dimensional transport of interacting particles: currents, density profiles, phase diagrams, and symmetries*, Phys. Rev. E **87** (2013), 062126.

[DJLS93] B. Derrida, S. A. Janowsky, J. L. Lebowitz, and E. R. Speer, *Exact solution of the totally asymmetric simple exclusion process: shock profiles*, J. Stat. Phys. **73** (1993), no. 5/6, 813–842.

[Ein05] A. Einstein, *Über die von der molekularkinetischen Theorie der Wärme geforderte Bewegung von in ruhenden Flüssigkeiten suspendierten Teilchen*, Ann. d. Phys. **322** (1905), no. 8, 549–560.

[Fam90] F. Family, *Dynamic scaling and phase transitions in interface growth* , Phys. A **168** (1990), 561–580.

[Fer92] P. A. Ferrari, *Shock fluctuations in asymmetric simple exclusion*, Probab. Theory Relat. Fields **91** (1992), 81–101.

[FLS77] R. P. Feynman, R. B. Leighton, and M. Sands, *The Feynman lectures on physics*, vol. 1, Basic Books, USA, 1977.

[FNW92] M. Fannes, B. Nachtergaele, and R. F. Werner, *Finitely correlated states on quantum spin chains*, Comm. Math. Phys. **144** (1992), no. 3, 443–490.

[Gib02] J. W. Gibbs, *Elementary principles in statistical mechanics*, 1902.

[Gil76] D. T. Gillespie, *A general method for numerically simulating the stochastic time evolution of coupled chemical reactions*, Journal of Computational Physics **22** (1976), no. 4, 403–434.

[GM06] O. Golinelli and K. Mallick, *Derivation of a matrix product representation for the asymmetric exclusion process from the algebraic bethe ansatz*, J. Phys. A.: Math. Gen. **39** (2006), 10647–10658.

[GT13] C. Graham and D. Talay, *Stochastic simulation and Monte Carlo methods*, Springer-Verlag, Berlin Heidelberg, 2013.

[HM09] P. Hänggi and F. Marchesoni, *Artificial Brownian motors: controlling transport on the nanoscale*, Rev. Mod. Phys. **81** (2009), 387–442.

[HMN05] P. Hänggi, F. Marchesoni, and F. Nori, *Brownian motors*, Ann. Phys. **14** (2005), no. 1-3, 51–70.

[HN93] V. Hakim and J. P. Nadal, *Exact results for 2D directed animals on a strip of finite width*, J. Phys. A: Math. Gen. **16** (1993), no. 7, L213.

[Isi25] E. Ising, *Beitrag zu Theorie des Ferromagnetismus*, Z. Phys **31** (1925), 253–258.

[KPZ86] M. Kardar, G. Parisi, and Y. C. Zhang, *Dynamic scaling of growing interfaces*, Phys. Rev. Lett. **56** (1986), 889–892.

[Kru06] J. Krug, *Boundary-induced phase transitions in driven diffusive systems*, Phys. Rev. Lett. **67** (2006), no. 14, 1882–1885.

[KSKS98] A. B. Kolomeisky, G. M. Schütz, E. B. Kolomeisky, and J. P. Straley, *Phase diagram of one-dimensional driven lattice gases with open boundaries*, J. Phys. A: Math. Gen. **31** (1998), 6911–6919.

[KSZ91] A. Klumper, A. Schadschneider, and J. Zittartz, *Equivalence and solution of anisotropic spin-1 models and generalized t-j fermion models in one dimension*, J. Phys. A.: Math. Gen. **24** (1991), no. 16, L955.

[MGP68] C. T. MacDonald, J. H. Gibbs, and A. C. Pipkin, *Kinetics of biopolymerization on nucleic acid templates*, Biopolymers **6** (1968), 1–25.

[MM03] S. Matthias and F. Müller, *Asymmetric pores in a silicon membrane acting as massively parallel brownian ratchets*, Nature **424** (2003), 53–57.

[MRR+53] N. Metropolis, A. W. Rosenbluth, M. N. Rosenbluth, A. H. Teller, and E. Teller, *Equation of state calculations by fast computing machines*, J. Chem. Phys. **21** (1953), no. 6, 1087–1092.

[NS92] K. Nagel and M. Schreckenberg, *A cellular automaton model for freeway traffic*, J. Phys. I France **2** (1992), 2221–2229.

[PS99] V. Popkov and G. M. Schütz, *Steady-state selection in driven diffusive systems with open boundaries*, Europhys. Lett. **48** (1999), no. 3, 257–263.

[Pur77] E. M. Purcell, *Life at low Reynolds number*, Am. J. Phys. **45** (1977), 3–11.

[Rei02] P. Reimann, *Brownian motors: noisy transport far from equilibrium*, Phys. Rep. **361** (2002), 57–265.

[RLS+99] S. Rice, A. W. Lin, D. Safer, C. L. Hart, N. Naber, B. O. Carragher, S. M. Cain, E. Pechatnikova, E. M. Wilson-Kubalek, M. Whittaker, E. Pate, R. Cooke, E. W. Taylor, R. A. Milligan, and R. D. Vale, *A structural change in the kinesin motor protein that drives motility*, Nature **402** (1999), 778–784.

[RSAP94] J. Rousselet, L. Salome, A. Ajdari, and J. Prost, *Directional motion of brownian particles induced by a periodic asymmetric potential*, Nature **370** (1994), 446–448.

[Sch01] G. M. Schütz, *Exactly solvable models for many-body systems far from equilibrium*, Phase transitions and critical phenomena (C. Domb and J. Lebowitz, eds.), vol. 19, Academic Press, London, 2001, pp. 1–251.

[SD92] G. Schütz and E. Domany, *Phase transitions in an exactly soluble one-dimensional exclusion process*, J. Stat. Phys. **72** (1992), no. 1/2, 277–296.

[Smo06] M. Smoluchowski, *Zur kinetischen Theorie der Brownschen Molekularbewegung und der Suspensionen*, Ann. d. Phys. **326** (1906), no. 14, 756–780.

[Smo12] M. Smoluchowski, *Experimentell nachweisbare, der üblichen Thermodynamik widersprechende Molekular-Phänomene*, Phys. Zeitschr. **13** (1912), 1069–1080.

[Spi70] F. Spitzer, *Interaction of Markov processes*, Adv. Math. **5** (1970), 246–290.

[Tho13] N. T. Thomopoulos, *Essentials of Monte Carlo simulation*, Springer-Verlag, New York, 2013.

[YE66] W. M. Young and E. W. Elcock, *Monte Carlo studies of vacancy migration in binary ordered alloys: I*, Proceedings of the Physical Society **89** (1966), no. 3, 735.

List of Figures

List of Tables

Acknowlegdement

First, I want to express my gratitude to Prof. Maaß for giving me the opportunity to work on this interesting thesis. Especially, I want to thank him for his patience, encouragements and advices.
I would also like to extend my sincere gratitude to Dr. Marcel Dierl. Without his guidance and support during this work, this thesis would not have been completed.
My thanks also goes to the whole work group Maaß for having a sympathetic ear to any questions I had and whenever I had problems.
Lastly, I want to thank my family for their support and continuous encouragement throughout my years of study.

Eidesstaatliche Erklärung

Ich versichere, dass ich die eingereichte Master-Arbeit selbstständig und ohne unerlaubte Hilfe verfasst habe. Anderer als der von mir angegebenen Hilfsmittel und Schriften habe ich mich nicht bedient. Alle wörtlich oder sinngemäß den Schriften anderer Autoren entnommenen Stellen habe ich kenntlich gemacht.

Ort, Datum	Unterschrift